The Astronomical Journal, 151:27 (20pp), 2016 February doi:10.3847/0004-6256/151/2/27

SEARCH FOR LOW-MASS OBJECTS IN THE GLOBULAR CLUSTER M4. I. DETECTION OF VARIABLE STARS

M. Safonova[1], D. Mkrtichian[2], P. Hasan[3], F. Sutaria[1], N. Brosch[4], E. Gorbikov[4], and P. Joseph[5]
[1] Indian Institute of Astrophysics, Koramangala 2nd block, Bangalore 560034, India; rita@iiap.res.in
[2] National Astronomical Research Institute of Thailand (NARIT), 191 Siriphanich Building, Huaykaew Road, Suthep, Muang Chiang Mai 50200, Thailand
[3] Department of Physics, Maulana Azad National Urdu University (MANUU), Hyderabad 500034, India
[4] Department of Astronomy and Astrophysics and the Wise Observatory, Tel Aviv University, Tel Aviv 69978, Israel
[5] Department of Physics, Christ University, Hosur Road, Bangalore 560029, India
Received 2015 August 21; accepted 2015 November 6; published 2016 January 22

ABSTRACT

With every new discovery of an extrasolar planet, the absence of planets in globular clusters (GCs) becomes more and more conspicuous. Null detection of transiting hot Jupiters in GCs 47 Tuc, ω Cen, and NGC 6397 presents an important puzzle, raising questions about the role played by cluster metallicity and environment on formation and survival of planetary systems in densely populated stellar clusters. GCs were postulated to have many free-floating planets, for which microlensing (ML) is an established tool for detection. Dense environments, well-constrained distances and kinematics of lenses and sources, and photometry of thousands of stars simultaneously make GCs the ideal targets to search for ML. We present first results of a multisite, 69-night-long campaign to search for ML signatures of low-mass objects in the GC M4, which was chosen because of its proximity, location, and the actual existence of a planet. M4 was observed in *R* and *I* bands by two telescopes, 1 m T40 and 18-inch C18, of the Wise Observatory, Tel Aviv, Israel, from 2011 April to July. Observations on the 1 m telescope were carried out in service mode, gathering 12 to 48 20 s exposures per night for a total of 69 nights. C18 observations were done for about 4 hr a night for six nights in 2011 May. We employ a semiautomated pipeline to calibrate and reduce the images to the light curves that our group is developing for this purpose, which includes the differential photometry package DIAPL, written by Wozniak and modified by W. Pych. Several different diagnostics are employed for search of variability/transients. While no high-significance ML event was found in this observational run, we have detected more than 20 new variables and variable candidates in the M4 field, which we present here.

Key words: globular clusters: general – globular clusters: individual (M4) – gravitational lensing: micro – stars: variables: general

1. INTRODUCTION

The field of exoplanetary studies has evolved considerably over the past few decades and is now one of the fastest-developing sciences, with 1800 planets confirmed and more than 4000 candidates discovered since 1995.[6] It is now believed (Cassan et al. 2012) that stars with planets are a rule rather than an exception, with estimates of the actual number of planets exceeding the number of stars in our Galaxy alone by orders of magnitude (including unbound, or free-floating, planets (FFPs); e.g., Strigari et al. 2012), super-Earths being the most abundant type. Our interest in exoplanets lies in the fact that, anthropically, we believe that life can only originate and exist on planets; therefore, the most fundamental interest is in finding a habitable planet—the Earth twin.

However, with every new discovery of an extrasolar planet in the field of the Galaxy, the paucity of planets in stellar clusters becomes more and more conspicuous. It may not be accidental that, with just a few exceptions, thousands of planetary candidates detected in the past several years all reside in the field of the Galaxy. Though most stars, including our Sun with its large planetary system, are born in stellar clusters, the scarcity of detected planets in both open clusters (OCs) and globular clusters (GCs) presents an important puzzle. Is environment important for formation and/or survival of planets? The usual reasons that are brought forward to explain the lack of planets in clusters are high stellar densities, leading to high interaction rate and disruption of forming planetary systems, or even inhibition of planetary formation due to the truncation of protoplanetary disks (see, e.g., Rosotti et al. 2014 and references therein). UV photoevaporation and supernovae (SNe)/stellar winds have also been suggested to inhibit and/or disrupt planetary formation (e.g., Bally 2003; Adams et al. 2004).

Null results in the dedicated searches in GCs 47 Tuc, ω Cen, and NGC 6397 (Gilliland et al. 2000; Weldrake et al. 2007, 2008; Nascimbeni et al. 2012) and only a handful of planets in OCs (Mochejska et al. 2006; Montalto et al. 2011) seem to confirm these theories. However, recent findings from observations of the OC NGC 6811 (Meibom et al. 2013) have turned the tide. The main conclusion of the study, based on the *Kepler* data, is that the frequency of stars with planets in OCs is consistent with the frequency of stellar hosts in the Galactic field. The study shows that planets can indeed survive the harsh conditions of clusters' early dense phase, SNe explosions, UV radiation, and stellar winds from young stars. Moreover, the existence of planets in multiple host systems (at least 57 planetary systems as of 2012; Roell et al. 2012) indicates that perturbations by neighboring stars do not efficiently inhibit planetary formation. *Kepler*'s discoveries of multiple planets orbiting multiple hosts show that such systems are actually common in the Galaxy (e.g., Di Folco et al. 2014; Horch et al. 2014; Roberts et al. 2015).

1.1. Free-floating Planets in GCs

In GCs, another reason for the absence of planets was proposed—low intrinsic metallicities of most Galactic

[6] Extrasolar Planets Encyclopedia, http://exoplanet.eu/catalog/

GCs. However, OCs of solar metallicity, NGC 6940 ([Fe/H] = 0.01; Chen et al. 2003), and of supersolar metallicity, NGC 6791 ([Fe/H] = 0.3; Boesgaard et al. 2009), were the subject of a number of transit surveys with null results, while the relatively metal-poor GC M4 ([Fe/H] ~ −1.2) hosts a planet. The search for planets in GCs was designed to only look for hot Jupiters, and hot Jupiters do seem to have strong dependence on host metallicity. Hot Jupiters are a special type of giant planets orbiting at distances of less than 0.1 AU and tidally locked to the parent star. The searches in 47 Tuc and ω Cen were based on the assumption that GCs have the same distribution of hot Jupiters as in the field. However, GCs have more evolved stars rather than Sun-like: K or M spectral types with mass of ~0.8 $M_{\odot}$ on average. In addition, transit methods are fraught with limitations such as stellar–noise (i.e., low-level variability), dependence on line-of-sight orientation, and the necessity to observe several transits for the firm confirmation. *Kepler*'s mission was successful because it was looking at nearby stars—most of the planets *Kepler* detected reside typically between about 100 pc and 1 kpc, while the distances to 47 Tuc, ω Cen, and NGC 6397 are ~5, 4.8, and 2.2 kpc, respectively. In addition, the orbital decay of transiting hot Jupiters over the GC age span could have resulted in their destruction (Jackson et al. 2009), leaving much fewer transiting planets, which alone can explain the lack of detected transits without invoking metallicity arguments (Debes & Jackson 2010).

In 2007 it was suggested that planets in low-metallicity systems do not reside at small orbital separations (Soker & Hershenhorn 2007), and thus the transit method is insensitive to them. Giant planets can still form at large radii from their low-metallicity hosts, but most wide-separation systems (>0.3 AU) will be disrupted due to tidal interactions with neighboring systems, which are expected to be very effective in dense GCs (Bonnell et al. 2001). Simulations by Parker & Quanz (2012) have shown that planetary systems with large a ~ 5–30 AU are likely to be disrupted by close passages of neighboring stars in the birth clusters at a rate of up to ~10%.

Tidal disruption of planetary systems in clusters (see Spurzem et al. 2009 and references therein) would lead to a population of FFPs. Using N-body simulations, Hurley & O'Shara (2002) showed that as many as 30% of planets in a typical GC could get liberated from their parent stars. A population of free-floating substellar objects has been detected in young open clusters (see, e.g., Lucas et al. 2001; Zapatero-Osorio et al. 2002; Haisch et al. 2010; Peña Ramírez et al. 2011), which more likely formed like stars but reside in planetary-mass range. Peña Ramírez et al. (2011) have recently identified a population of planetary-mass objects in the σ Ori cluster and suggested that they could be as numerous as brown dwarfs. This also indicates that there could be a population of such objects in the solar vicinity, both in the field and in young moving groups and clusters. In 2012, a 4–7 $M_{\rm J}$ FFP was discovered at 30 pc from Earth, belonging to the young moving group AB Doradus (CFBDSIR2149-0403; Delorme et al. 2012), and in 2013, a 6 $M_{\rm J}$ FFP at 24 pc from Earth in the Beta Pictoris moving group (PSO J318.5-22; Liu et al. 2013). Out of all exoplanets, FFPs are especially interesting because, like cosmic wanderers, they may be the source of life, spreading seeds of life throughout the Galaxy (e.g., Stevenson 1998; Durand-Manterola 2010). According to recent estimates (Strigari et al. 2012), their number in our Galaxy may exceed the number of bound planets, and FFPs are expected to be a common product of most planetary formation scenarios (Bennett et al. 2007).

FFPs in clusters can be formed through several different channels. FFPs of Jupiter mass can form by collisions between high-mass protoplanetary disks if the stellar densities are high (Lin et al. 1998), as is the case for GCs. They could be scattered from already-formed planetary systems by dynamic interactions in the multiple-planet system or in multiple-star systems (e.g., Veras & Raymond 2012; Ford 2014), or kicked out by interaction of the system with a passing star, especially if they reside at large orbital separation. They could have been kicked out from the system during a parent star's mass loss in the end of stellar life (Veras et al. 2011), especially planets as orbitally distant as several hundred AU. Planets could have been formed in situ by direct collapse like stars or from the cometary blobs (CBs—remnants of SN explosions as suggested by Dado et al. 2011) and could represent the low-mass tail of the stellar initial mass function (IMF; (Veras & Raymond 2012).

Several circumstantial pieces of evidence point to existence of planets in GCs:

1. Demonstration by Ida & Kokubo (2004) that protoplanetary disks with lower than solar metallicity can form many terrestrial planets; perhaps as many as 50–100 per star (Hurley & Shara 2001).
2. Report that the so-called "second parameter" problem of the horizontal brach (HB) morphology in GCs can be resolved by assuming the "planet second parameter" model, where the planetary formation in GCs can in fact be very efficient at the time when the GCs were forming (Soker & Hadar 2001). Incidentally, the authors noted that 47 Tuc would not have hot Jupiters due to the paucity of blue HB stars in that cluster, and that the clusters with a higher value of HBR index shall be expected to have planets around many main-sequence (MS) stars.
3. Association of several previously detected microlensing (ML) events in the bulge with few GCs (de Luca & Jetzer 2008). It was shown that the modeling does not rule out lensing of the bulge stars by the substellar objects in these clusters.
4. Absence of an obvious correlation between the metallicities of the host star and the presence of low-mass planets (Buchhave et al. 2012).
5. Existence of planets orbiting metal-poor old stars, sometimes as old as 11.2 ± 1.0 Gyr (e.g., Kepler-444; Campante et al. 2015).
6. Actual existence of a planet in the metal-poor GC M4—PSR B1620-26 b. This planet was probably formed through gravitational instability in a circumbinary disk of a pulsar–white dwarf progenitor as a result of an interaction with a passing MS star—the formation scenario that is insensitive to the metallicity (Beer et al. 2004).
7. Discovery of an Li-rich star in M4 (Monaco et al. 2012). One possible explanation of Li content higher than normal for Population II stars was recently suggested for the case of a red giant field star, BD+48740 (Adamów et al. 2012), which has at least one planet—that a star ingested a planet. Li is preserved in relatively cold environments of planets as they form. A planet absorbed

by a star would deliver Li to its atmosphere. The primordial level of Li in M4 star no. 37934 could be a hint that the star has (or had) planet(s).

8. Demonstration by observational analysis and theoretical modeling that a hard X-ray transient near the center of the GC NGC 6388 is strongly consistent with a tidal disruption of a free-floating terrestrial planet by a massive white dwarf (Del Santo et al. 2014).

2. MICROLENSING IN GCs

Since FFPs are not bound to a star, they are undetectable by any of the traditional searching methods, transit or radial velocity (RV); thus, it is necessary to employ other techniques. Gravitational ML is already established as an additional tool in detecting extrasolar planets; moreover, it is the only way to detect the population of FFPs in GCs as their direct imaging is also not possible.

First, FFPs were detected by ML in 2011 (Sumi et al. 2011), which was the basis for the Strigari et al. (2012) estimates. However, the ML method to search for planets is not devoid of difficulties due to several factors. At any time, only some out of $\sim 10^6$ Galactic bulge stars are microlensed with sufficient magnification, and if such an event is due to a foreground planet, it is usually of a very short duration due to a small planetary Einstein radius, $R_E \sim 1$ day, even for a giant planet ($\sim 10^{-3}\ M_\odot$). Einstein radius R_E of the lens defines the region of high amplification, and the timescale of the event t_E is defined as the time it takes a source to cross the Einstein radius R_E,

$$t_E = \frac{2R_E}{v_t} = \frac{4}{v_t c}\sqrt{\frac{GM_L D_L (D_S - D_L)}{D_S}}. \quad (1)$$

Here M_L is the lens mass, D_L and D_S are the observer–lens and observer–source distance, respectively, and v_t is the lens transverse (to the line of sight) velocity. It can be seen that duration decreases as $\sqrt{M_{\rm planet}}$, thus demanding a very high cadence of observations. This may change with the launch of the Microlensing Planet Finder (MPF; Bennet et al. 2010). There is still the problem of a mass–distance degeneracy, as ML observations allow the measurement of only two observables, the timescale of the event and the amplification at maximum. In most cases the lens is not seen, and therefore D_L cannot be independently determined. If, for example, one has measured a certain timescale of 1 month, it could be due to either large M_L and small v_t or small M_L and large v_t. Several methods were suggested and are being used to resolve this degeneracy, which essentially requires the breaking of the symmetry of a standard Paczynski light curve (see, e.g., review in Sutherland 1999, but not exclusively).

Here we suggest that observing GCs for ML by FFPs belonging to the cluster can, in principle, resolve this degeneracy and that, with carefully arranged observational setup, such planets can be detected from the ground. GCs present ideal targets for the dedicated ML searches—their compactness allows observations of thousands of stars in a single exposure in a single frame, which maximizes the temporal coverage and increases the probability of detection. Events produced by planetary lenses are only of a few days duration for a giant planet (see Section 3); therefore, it is sufficient to observe a cluster for several consecutive nights. A good general knowledge of GCs—stellar kinematics, metallicity, age and distances, relative inhomogeniety in many parameters, and a history of formation from the same initial cloud (same IMF) provides means of resolving the mass–distance degeneracy, offering the only possibility to constrain their numbers and masses. Though the Einstein radius of an FFP event is small, given the perfect alignment, the ML signal —the high-amplification event—even from low-mass planets can be quite strong. We expect no light contribution from the lens, and provided that foreground stars are constant, the contribution of any foreground star will be canceled out in delta flux (ΔF) measurements,

$$\Delta F = F_{\rm base} A(u(t)) - F_{\rm ref}, \quad (2)$$

where $F_{\rm base}$ is the baseline (unmagnified) flux of a star undergoing amplification, $F_{\rm ref}$ is the flux of that star on a reference frame (RF), and $u(t)$ is the time-dependent impact parameter—the distance between the source and the lens in terms of Einstein radius. Amplification governs the shape of the ML light curve,

$$A(u(t)) = \frac{u^2 + 2}{u\sqrt{u^2 + 4}}. \quad (3)$$

High-amplification events occur when u is small ($u \ll 1$). For $0.05 \leqslant u \leqslant 0.02$, amplification can be 20 to 50, corresponding to a maximum increase in brightness of 3 to 4 mag.

FFPs behave like low-mass stars evaporating into the cluster's halo, especially in the presence of strong tidal interactions (Spurzem et al. 2009) during a cluster's passage through the Galactic plane. Fregeau et al. (2002) performed the numerical simulations of the mass segregation in two-component star clusters and found that low-mass objects in the cluster halo can dominate the ML optical depth—for some initial conditions, the optical depth in the halo could be much greater than that of the luminous stars. Many GCs are known to exhibit tidal trails and halos (e.g., Leon et al. 2000), and it is possible that these trails contain FFPs detectable by wide-field surveys.

3. TARGET CLUSTER

M4 (NGC 6121) is the closest GC to the Sun at ~2 kpc. It is a very bright ($V = 5.9$ mag), relatively sparse, relatively metal-poor ([Fe/H] ~ -1.2) cluster projected near the edge of the Galactic bulge. The line of sight to M4 passes through the Galactic inner halo or, perhaps more correctly, the inner Population II spheroid, and the distant field stars may belong to the bulge or inner halo. The far side of the Galactic bar is also projected into the same Galactic quadrant as M4. We expect only a small number of foreground disk stars in our field, but there are a large number of background stars that can serve as sources for an ML event.

M4 is an interesting cluster in several ways. First, it hosts the only planet ever discovered in a globular cluster, PSR B1620-26 b (Richer et al. 2003). Second, the high ratio of a cluster age to the half-mass relaxation time strongly suggests that the cluster had experienced a core collapse, of which, however, there is no observational evidence (Richer et al. 2004). Therefore, M4 is expected to have an internal energy source capable of preventing core collapse. One candidate for this is primordial binaries, though the detected fraction of such objects is currently very low. The central M4 binary fraction is ~2%, compared to ~5.1% in the similar (in most parameters) NGC

Table 1
Relevant Parameters of M4

Distance from the Sun D_L	1.8 kpc
Central velocity dispersion σ_0	4 km s^{-1}
Proper motion $\dot{\phi}$	23.4 mas yr^{-1}
Diameter D_{GC}	42 pc
Distance to the bulge D_S	8.2 kpc

6397 (Richer et al. 2004; Davis et al. 2008), or to ∼22% and ∼21% in prototypical core-collapse clusters M71 and NGC 362, respectively.

M4 has a well-developed mass segregation (Richer et al. 2004) and a highly eccentric (0.88; Allen & Santillan 1993) chaotic orbit with galactocentric distance ranging from 0.5 to 6.9 kpc at each passage, resulting in the M4 population being strongly affected by tidal interactions with the Galactic disk. Due to the strong tidal stripping, M4 is expected to have a low-mass star deficiency. However, Richer et al. (2004) have calculated the number of stars at the hydrogen limit 0.085 $M_\odot$ to be from 14 to 49, concluding that if the slope of the cluster's mass function is unchanged down to the end of the MS, then there should be at least a few tens of MS stars at the faint end of the M4 field. They, however, found only six at $M \simeq 0.1\ M_\odot$ (Richer et al. 2004). The existence of a minimum stellar mass is a fundamental theoretical result that can in principle be confirmed by ML.

Since the cluster is situated very close to us, the majority of objects of interest would most probably belong either to M4 or to the bulge; therefore, we consider only these locations. To determine the cadence of observations, we assume that the lens belongs to the cluster and calculate the timescales of possible planetary ML events for two scenarios: (A) the source is a bulge background star, and (B) the source is a star within the cluster—a case of self-lensing. The relevant parameters for M4 are presented in Table 1.

1. Scenario A. The source is a bulge background star. In Jetzer (2015) four possible ML events were associated with the lenses in GCs seen against the background of the Galactic center. Following Equation (4) in Paczyński (1994), we calculate the time duration of the event t_E for a low-mass star of 0.1 $M_\odot$, a brown dwarf of 0.07 $M_\odot$, and a Jupiter of 0.001 $M_\odot$ to be 8.65 days, 7.33 days, and ∼1 day, respectively.
2. Scenario B. The source is a star within the cluster. The rate of self-lensing events in GCs was discussed in Safonova & Stalin (2010). The equation for the timescale reduces to

$$t_e = 48.6\left(\frac{10\ \mathrm{km\ s^{-1}}}{\sigma}\right)\left(\frac{M_L}{M_\odot}\right)^{1/2}\left(\frac{D_{LS}}{1\ \mathrm{Kpc}}\right)^{1/2}, \quad (4)$$

where D_{LS} is the lens—source distance, which we take to be the diameter of the cluster, D_{GC}. For the same three cases as in scenario A, we find the following timescales: 7.87 days for a low-mass star, 6.65 days for a brown dwarf, and about 19 hr for a Jupiter.

The details of the calculations will be presented in a separate communication (M. Safonova et al. 2015, in preparation).

4. OBSERVATIONS

Given the values of the timescales estimated in the previous section, it was decided to perform photometric monitoring of the cluster for about 4 months. As the lensing curves are achromatic, to distinguish from variations due to other phenomena, we carried out observations in two filters (I and R band) several times a night (when possible) in short exposures to avoid saturation of bright cluster stars. In addition, observing M4 with a wide-field telescope with field of view (FOV) larger than or at the tidal radius (∼22′) offers the opportunity to search for FFPs in its halo, especially with a background rich in stellar objects. Keeping that in mind, we supplemented the T40 observations with six nights on a wide-field C18 telescope with FOV of >1 square degree.

The main observational run was performed with the 1 m telescope (T40) of the Wise Observatory, Tel Aviv, Israel, from 2011 April 06 to July 07 in service mode, gathering 12–48 20 s exposures per night for a total of 69 nights in R and I filters. We have used R and I because the CCD's quantum efficiency is ∼40% between R and I and only about half of that in V. The field analyzed here is one out of four LAIWO[7] mosaic CCD fields (Figure 1, top) monitored during the run, CCD chip 2, which itself consists of four quadrants (nos. 5–8; Baumeister et al. 2006; Gorbikov et al. 2010). The size of each quadrant is 1048 × 1048 pixels, with a plate scale of 0.″87 pixel^{-1} (equivalent to a total FOV of ∼14.′5 × 14.′5). The cluster was positioned on quadrant 8, since it has the best characteristics (Figure 1, bottom).

Supplementary observations were performed with the 0.46 m Centurion 18 (C18) telescope, situated in the same area. It is equipped with a large-format CCD camera—STL-6303 of SBIG. Observations were performed remotely. The CCD (Brosch et al. 2008) has 3072 × 2048 pixels with a pixel scale of 1.″47 pixel^{-1}, giving a total FOV of 75′ × 50′. In the unbinned mode the readout noise is 15 electrons and the gain is 1.379 e ADU^{-1}. The observations were done for six nights from May 28 to June 02, for about 4 hr each night, gathering a total of 425 60 s exposures in R and I filters.

5. DATA REDUCTION AND SEARCH FOR TRANSIENTS

5.1. Basic Data Reduction

5.1.1. T40 Telescope

Since the readout noise and gain were different for each quadrant, we have calibrated them separately. All images were subjected to the basic data reduction (bias subtraction and flat-fielding) using the modular pipeline based on IRAF[8] scripts being developed by our group. The first module of this pipeline separates the frames based on the CCD image type identifier (bias, flat, object) into the corresponding lists, checks the quality of the images using the image statistics (and rejects "bad" frames), and edits the image headers with necessary information. The second module performs the basic reduction and creates the lists for the next processing. We did not make a separate dark current correction; the dark current has been found to be negligible for the exposure times used. Flat fields were constructed from dithered images of the twilight sky, and

[7] Large Area Imager for the Wise Observatory.
[8] IRAF is distributed by the National Optical Astronomy Observatory, which is operated by the Association of Universities for Research in Astronomy, Inc., under a cooperative agreement with the National Science Foundation.

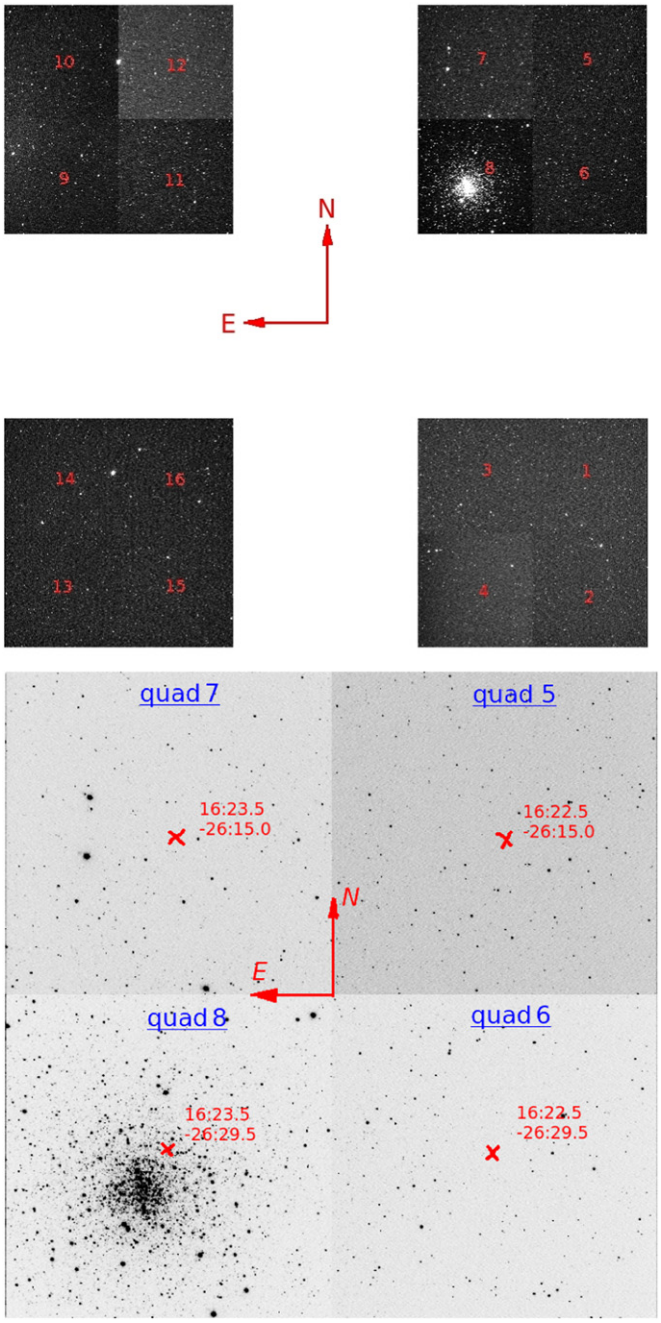

Figure 1. Top: LAIWO mozaic of M4 field. Bottom: LAIWO CCD chip 2 with M4 position on quad 8.

any star images were removed by combining flats in each color using a median filter. The sky flats were also used to correct for large-scale illumination variations in some quadrants (quad 5 and quad 7). A 25-pixel smoothing box was applied to the combined flats to erase the possible effects of any irregularities and leave only the large-scale pattern before processing the object frames. We did not use the cosmic-ray removal module of our pipeline, since the Difference Image Analysis Package (DIAPL) we have used in this work[9] has an option for cosmic-ray removal at the subtraction stage.

[9] We have used the version of DIAPL (Wozniak 2000) modified by W. Pych. This package is available at http://users.camk.edu.pl/pych/DIAPL/.

Because the exposure time was only 20 s, to increase the signal-to-noise ratio, we co-added up to six images taken sequentially within 1 hr on each night. We thus obtained a time series of frames where one night was represented by one or, occasionally, up to four data points. The co-adding was performed using DIAPL code *template.bash*, which assigns the time stamp of the first image of the stack to the final image. After co-adding, the resultant time series were moved to separate directories, one for each filter.

5.1.2. C18 Telescope

All images were subject to the same basic data reduction (bias subtraction and flat-fielding) using the same modular pipeline as for the T40 telescope, except that we have used the dark current subtraction option in the pipeline. We did not co-add the frames since we were looking for the short-term variability in this run. The preprocessed images were combined by filter and subjected to the same DIAPL in the search for variability.

5.2. Search for Variability

To extract the photometric variability, we have employed the differential imaging analysis (DIA) method, which showed excellent results when applied to the large data sets, and especially in crowded stellar fields (e.g., Alard & Lupton 1998; Wozniak 2000). DIA is sensitive to ML events even when the source star is too faint to be detected at the baseline. In this method, the so-called RF is constructed from images with the best seeing parameters. Next, a convolution kernel, representing the difference between the stellar point-spread functions (PSFs) of the RF and all the frames in the time series, is applied to the RF to match each of the images in the series. Finally, a convolved RF is subtracted from each image in the series. This allows for the elimination of all nonvariable stars in the resulting difference frames. If there is no difference in flux between the images, the residual frames are theoretically flat, while the variable or transient objects show up as positive or negative star-like residuals. The light curves for the variables are then extracted by the application of PSF photometry to the difference frames.

5.2.1. T40 Telescope

To reduce the effects of PSF variability, all frames were subdivided at the subtraction stage into overlapping subframes, depending on the number of stars in each quadrant. Quad 5 was not split at all, quad 6 and quad 7 were split into 2×2 subdivisions (524×524 pixel size), and quad 8 (where most of the cluster was located) was split into into 5×5 (209×209 pixel size) and into 4×4 (262×262 pixel size) subframes, as in the first case we found that some variables were lost between the subframes borders.

RFs for each quadrant were constructed by combining several (depending on the quadrant) co-added images with good seeing and low background. The combined frames were remapped to the RF coordinate system, and the convolved RF was subtracted from each frame in the time series (for details of the algorithm, see Wozniak 2000). The residual frames (difference images) were searched with IRAF DAOFIND for the presence of any positive stellar-like residuals, each subdivision separately. Regions at the locations of saturated stars were masked to remove them from the search. Since the

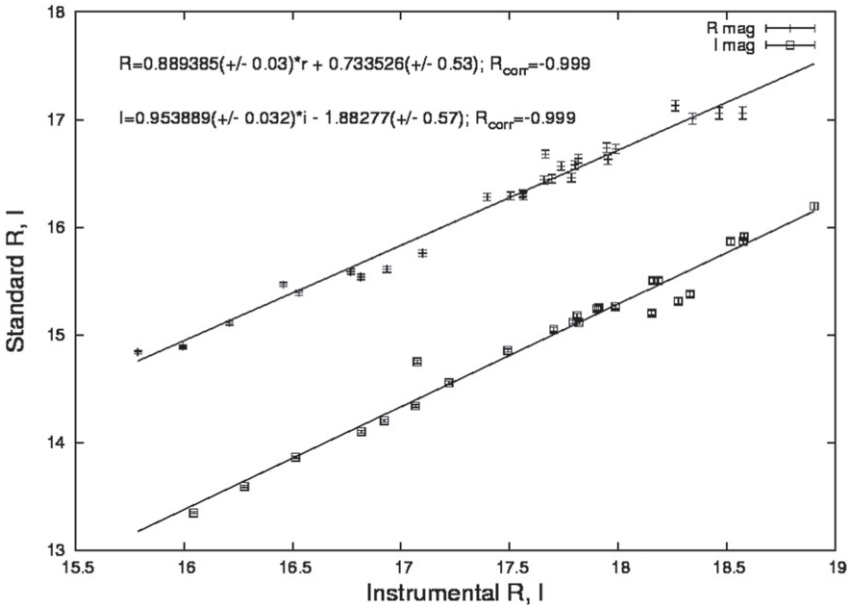

Figure 2. Photometric calibration of quad 5. *R* and *I* magnitudes are from the PPMXL'10 catalog.

stars undergoing the light variation show different brightness on each of the residual images, it was difficult to determine their central coordinates accurately; there was a slight constant positional variability of their PSF. To solve this problem, the pixel coordinate lists of detected residuals on every frame were "dumped" into one total list (IRAF task *txdump*). Each source was assigned a unique ID number by the *daofind* task, and we used this ID for all subsequent lists and databases. Concatenation of the coordinates from each subtracted frame was done by a Fortran code that searched for the nearest neighbors (within a specified radius of, say, 5–10 pixels) and averaged the centroid. The DIAPL photometry was performed on this final coordinate list, and the light curves were extracted in units of difference counts on subtracted images and examined by eye. The coordinates of the stars whose light curves were showing interesting variation were fed into the IRAF task *phot* to extract their aperture photometry on the RFs. These measurements were used to obtain the light curves in instrumental magnitudes by DIAPL.

For the light curves in which light variation was found, several methods were employed to find the best-fitting period: phase minimization method (PDM) using IRAF (*astutil* package), period determination code based on the Lomb–Scargle (LS) method, and the power spectrum analysis (Press et al. 2002), where the LS period is subsequently passed on to the code based on the algorithm of Lafler & Kinman (1965; LK method) and the light curves are phased out. Final analysis was performed using the open-source PerSea 2.1 package (Maciejewski 2005), which is based on the optimal analysis of the variance period search method of A. Schwarzenberg-Czerny (1989) and allows the automated variability type assignment.

5.2.2. C18 Telescope

The image frames were split into 8×6 subdivisions (424×324 pixel size), and RFs in both filters were constructed from only nine best frames from May 29, to minimize the chance of having an ML event in these frames. The rest of the methodology was as for the T40 telescope.

6. ASTROMETRIC AND PHOTOMETRIC CALIBRATION

6.1. T40 Telescope

Astrometric solution of each quadrant's RF was performed using two methods. Each quadrant's RF was loaded into the Aladin Sky Atlas (Bonnarel et al. 2000) with a corresponding field from *Hubble Space Telescope* (*HST*) cataloged images, and bright, but not saturated, stars were matched between the frames. We have used about 26 stars from all over the field and far from the center to perform this transformation. Each thus-calibrated RF was checked by loading the all-sky catalogs PPMXL (Röser et al. 2010; http://vo.uni-hd.de/ppmxl) and Two Micron All Sky Survey (2MASS; Skrutskie et al. 2006) and for all quadrants but quad 6, the accuracy was within 1″. Quad 6 was rotated and scaled down; therefore, for this quadrant we have used IRAF astrometric calibration utility. No less than 20 standard stars from the online catalog by Stetson (2000) at the Canadian Astronomical Data Center (CADC)[10] uniformly distributed around the quadrant center were identified, and the list of their (x, y) and (R.A., Decl.) coordinates was created. This list was an input to the *ccmap* task of the *imcoords* package in IRAF. The obtained accuracy was 0.″0678 in R.A. and 0.″0437 in Decl. The task *ccsetwcs* was used to update the header of the quad 6 RF in the J2000 epoch.

The same Stetson's photometric standards were used to obtain the absolute photometric calibration. For stars whose standard *R* magnitudes were not available in the Stetson (2000) catalog, data from the PPMXL'10 catalog were used. The photometric solution was obtained by linear fitting the standard magnitudes versus instrumental magnitudes. The resultant solutions (with correlation coefficient of the fit $R \sim 1$) were applied to the instrumental magnitudes of variable stars to obtain their standard $\langle R \rangle$ and $\langle I \rangle$ magnitudes. In Figure 2 we

[10] The catalog is available at http://www3.cadc-ccda.hia-iha.nrc-cnrc.gc.ca/community/STETSON/standards/.

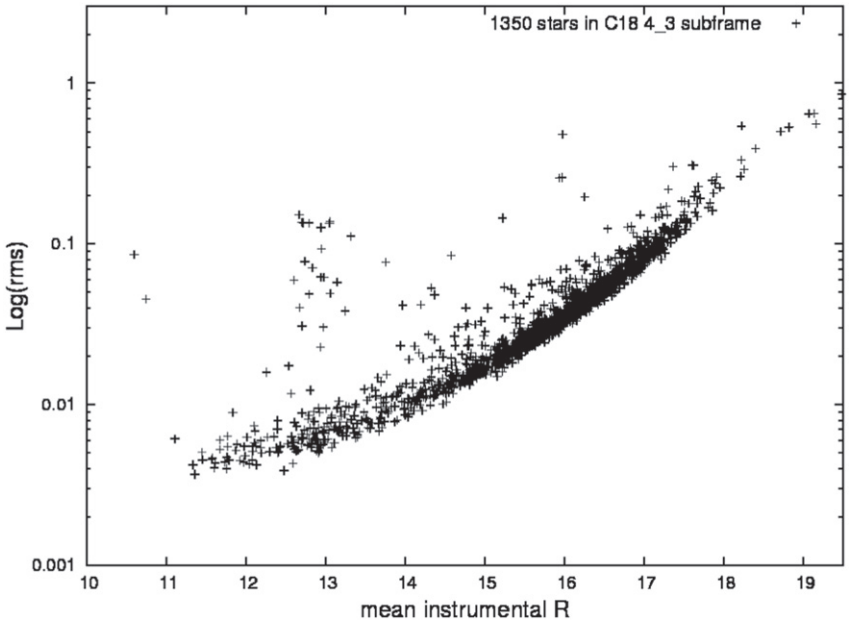

Figure 3. Photometric accuracy of the central part of C18.

show as an example the fit for quad 5, both *I* and *R* filters. We have not found any color dependence here.

6.2. C18 Telescope

The same approach was applied to the central subdivision 4_3 (Section 5.2.1) of the C18 RF, except that here we used *R* and *I* magnitudes given in Stetson's catalog. The photometric solution was found for 29 Stetson standard stars, and the solution was applied to the instrumental magnitudes of all stars in this subsection. We have found a small color dependence, which was included in the fitting:

$$\begin{aligned} R - r &= -0.167651(R - I) - 0.20271, \\ I - i &= -0.137662(R - I) - 0.887425, \\ R - I &= 0.861806(r - i) + 0.670682, \end{aligned} \quad (5)$$

where *R*, *I* are standard magnitudes and *r*, *i* are instrumental magnitudes. In Figure 3 we show the plot of standard deviation (rms) versus the mean instrumental *R* magnitude for this subsection. We used the light curves for all detected (~1350) stars in the 4_3 *R* filter subframe of the RF. We can see that our photometric limit is about 19 mag.

7. VARIABILITY IN THE FIELD OF M4

7.1. Stars Previously Reported as Variables

M4, being the closest GC to us, has been the subject of quite intense attention in the past few years, both from the ground (e.g., Kaluzny et al. 2013; Stetson et al. 2014) and from space (Nascimbeni et al. 2014). In spite of that, a few puzzling facts still remain. For example, there are no SX Phe-type stars firmly confirmed in the cluster. Yao (1993) proposed one star as an SX Phe, reporting it to be a blue HB star; however, it is located in the wrong place on the cluster's color–magnitude diagram (CMD) and does not seem to even be variable (Yao & Uloa 1993; Stetson et al. 2014). Kaluzny et al. (2013) have reported four SX Phe stars, two possible cluster members, and two possible field stars; the cluster members were subsequently found to be most probably nonvariable, and one possible nonmember, though confirmed to vary with SX Phe-like period (0.04088 days), to be too faint to be indeed a cluster's SX Phe star ($V = 19.3$; Nascimbeni et al. 2014). Several groups searched for cataclysmic variables (CVs/DNe) and found

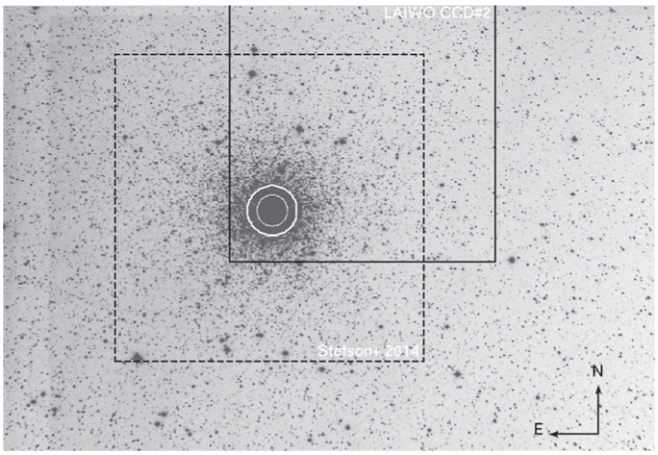

Figure 4. *R*-band reference frame of C18. Overlayed are the FOV of Stetson et al. (2014) (dashed black square) and the LAIWO CCD#2 FOV (solid black square). The small white circle is the FOV of the *HST* study (Nascimbeni et al. 2014). The larger solid white circle depicts the M4 core size ($r_c = 1'.16$).

Table 2
Identification of Stars V54–V60

Clement ID	Greenstein No.	Alcaino No.	Lee ID	(R.A. Decl.) 2000.0
V54	G30	···	L3621	16:23:42.84 −26:29:28.0
V55	G327	A64	L3315	16:23:45.94 −26:23:37.1
V56	G265	A375	L4508	16:23:45.98 −26:33:39.4
V57	G266	···	L4509	16:23:46.98 −26:33:44.4
V58	G206	A491	L4632	16:23:47.87 −26:32:06.4
V59	G481	A371	L4512	16:23:50.18 −26:33:24.4
V60	G543	A376	L4507	16:23:45.26 −26:33:57.3

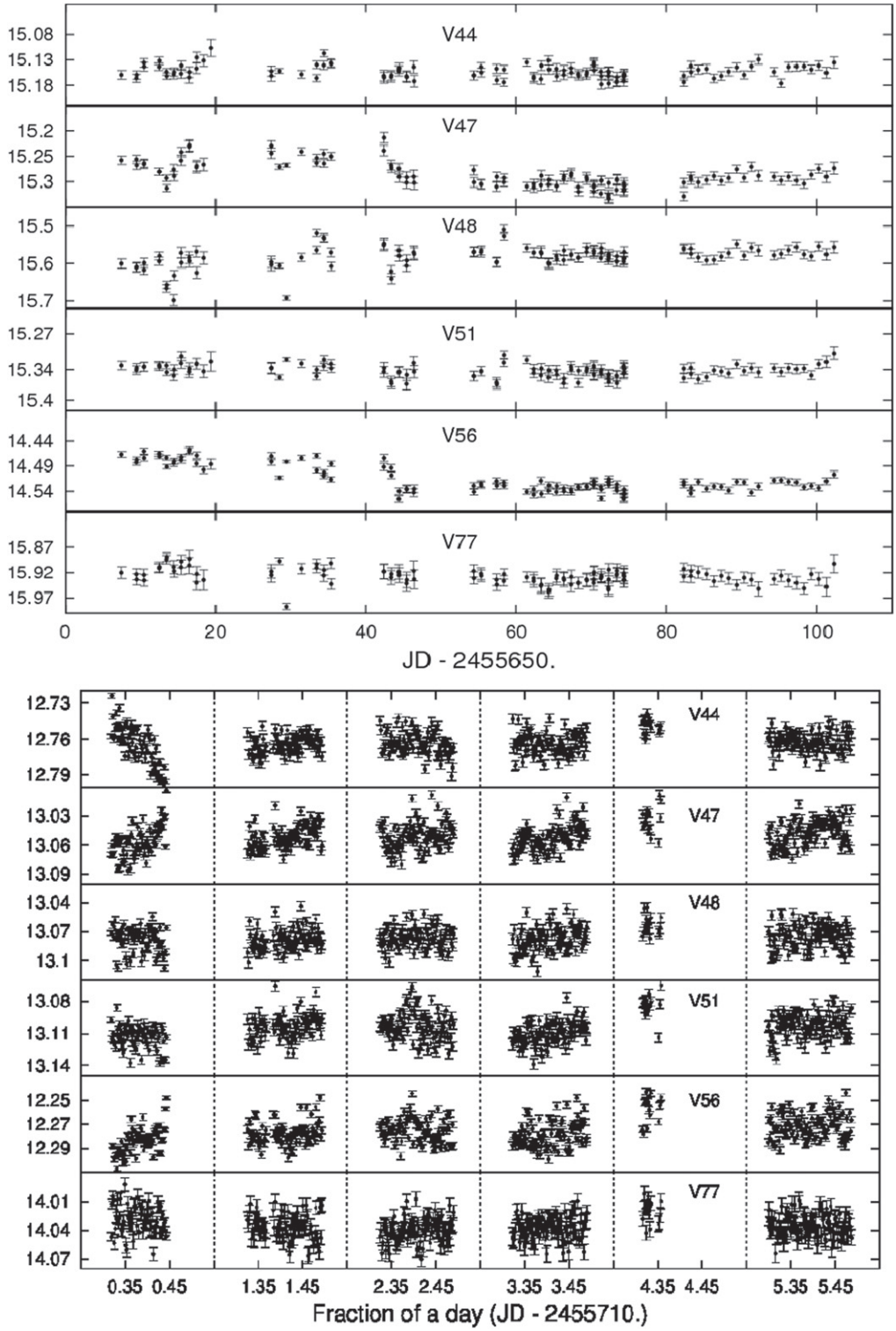

Figure 5. T40 (top) and C18 (bottom) time-domain light curves of variables V44, V47, V48, V51, V56, and V77 in instrumental *R* magnitudes. Names are given in the plots.

none. Only two variable blue straggler stars (BSS) were found, one by Kaluzny et al. (1997), and another only recently by *HST* observations (Nascimbeni et al. 2014), both eclipsing binaries. Although we cannot compete with the superior spatial resolution of the *HST*, which detects photometric variability on the order of a few hundredths of magnitude, our present study complements the *HST* study in having a much wider FOV (see Figure 4). We, in addition, obtained a good photometry in *R* and *I* for bright stars, such as a cluster's RR Lyrae, a subject of the Stetson et al. (2014) study. We also have a time series suited well for investigating both the long-period variables (LPVs, ∼4 months on the T40 telescope) and a short-period variable (SPV, six nights on the C18 telescope).

The newly updated Christine Clements online catalog (last update 2015; Clement et al. 2001) lists now 111 variables, including recent findings by Kaluzny et al. (2013) from

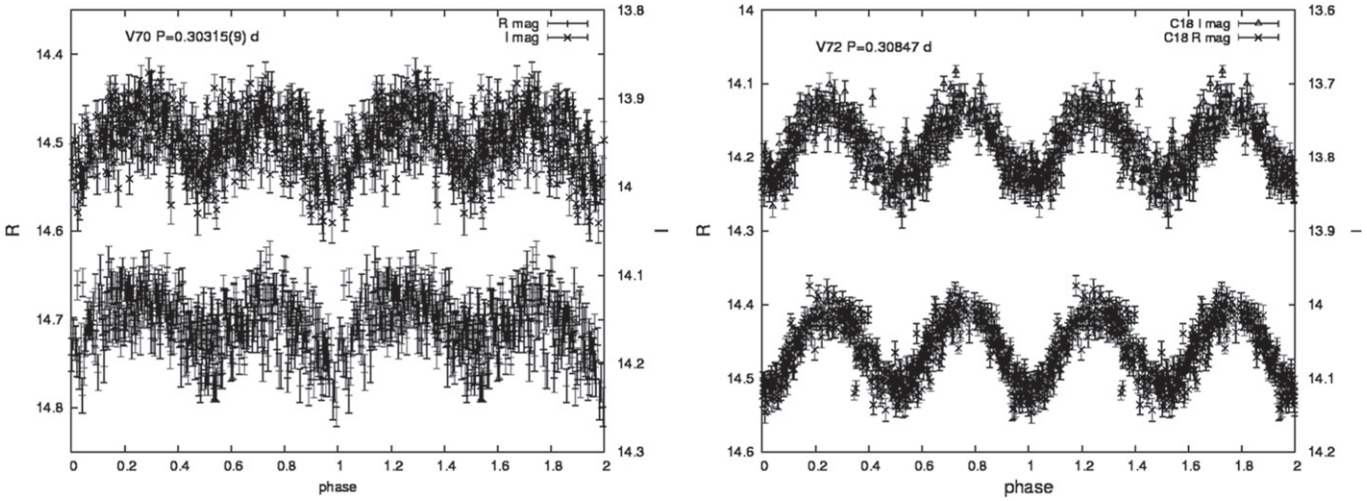

Figure 6. C18 phase curves of V70 and V72 in standard R and I magnitudes.

Table 3
SX Phe Stars in M4 Suggested by Kaluzny et al. (2013)

Kaluzny	$P_{\rm Kal}$	Stetson et al. (2014)	*HST* Study (2014)	This Work	
ID	Days	Result	Result	T40	C18
K61	0.0413287	non-var?	did not detect	LP?	blended with bright $V = 13.165$ neighbor; cannot get light curve
K68	0.0380887	non-var?	did not detect	noisy; LP?	not phasing at $P^{\dagger}_{\rm Kal}$

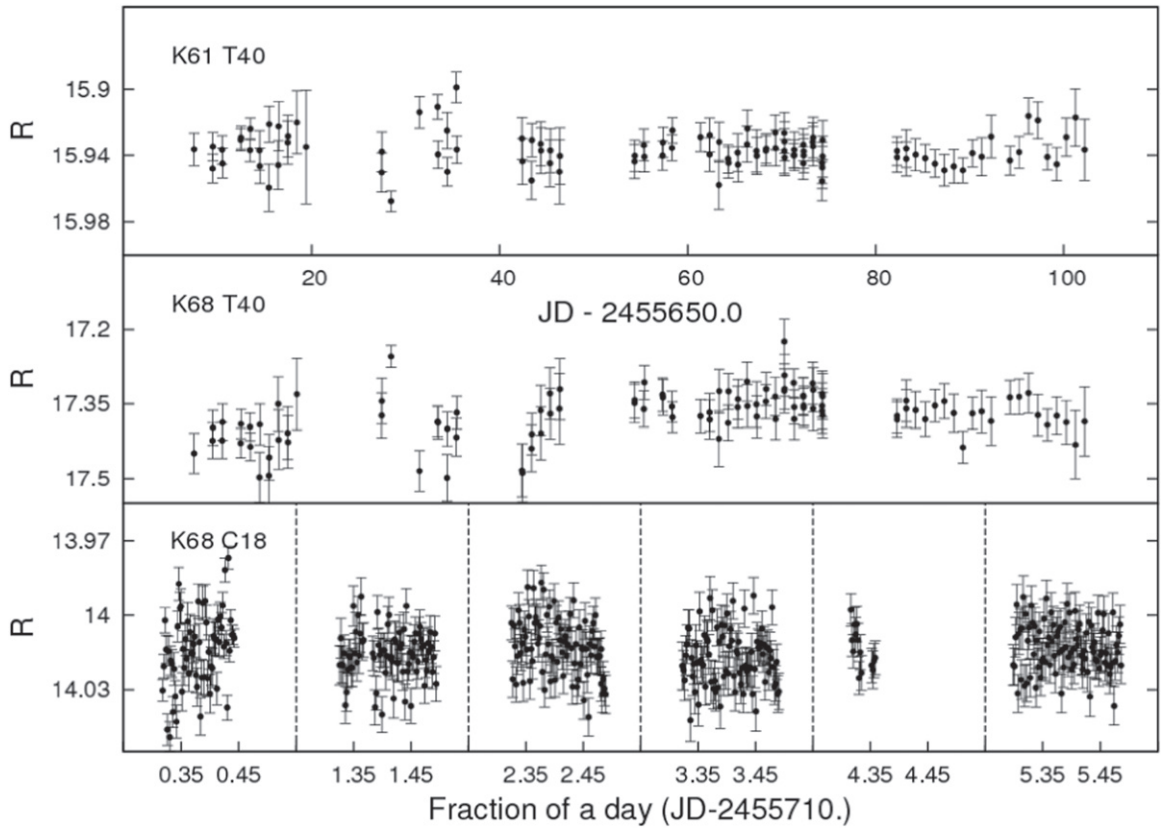

Figure 7. T40 and C18 time-domain light curves of K61 and K68 in instrumental R magnitudes. Top: T40 light curves of K61. Middle and bottom: T40 and C18 light curves of K68, respectively.

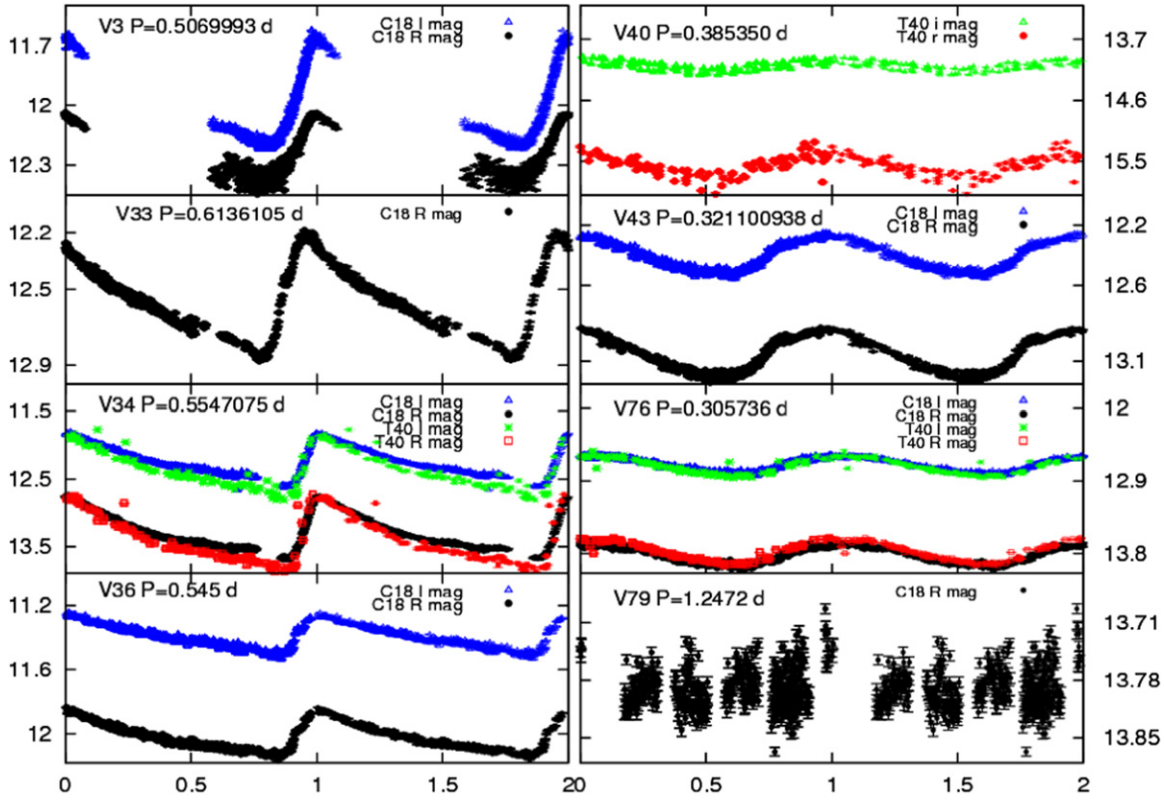

Figure 8. C18/T40 light curves of V3, V33, V34, V36, V43, V76, and V79 in standard magnitudes. C18 light curves of V40 are given in instrumental magnitudes (see text). Names and respective periods are given in the plots. The color coding is as follows: blue—C18 *I*mag; black—C18 *R* mag; green—T40 *I* mag; red—T40 *R* mag.

the Clusters AgeS Experiment (CASE), Nascimbeni et al. (2014), and Stetson et al. (2014).

In this paper we use the variable star identifiers given by Clement et al. (2001). Variables from CASE were named K with some number, and the cross-match with other group's identifiers was performed. In this paper we only report the newly found variables/variable candidates and our findings on those previously reported variables that "brought out something new" (where possible).

We have recovered all variables listed in Clement's catalog of 2009 (80 variables at the time of observations), except V4, V13, and V53, as they were saturated on both telescopes. In Clement's catalog, some variables did not have their coordinates defined (V53–V61; only *x*, *y* positions were given). The LAIWO quad 8 RF was compared and contrasted to the ID charts of Greenstein (1939), Alcaino (1975), and Lee (1997), and the coordinates of seven variables were located, identified by the assigned name, and their positions verified. We found their coordinates by triangulating their position on at least two of these ID charts. Their equatorial coordinates were found using the Aladin Sky Atlas and the *cctran* task of the *imcoords* package in IRAF with an accuracy of $<0\farcs1$. These stars, with their coordinates and the cross-matches, are presented in Table 2.

Incidentally, Stetson et al. (2014) also reported searching for these missing data and successfully identified them by plotting their predicted positions on their stacked image and finding the closest bright star to each position. They misidentified only one star, V57, and we have confirmed it by verifying with the online Samus et al. (2007–2015) catalog.

7.2. New Data on Previously Reported Variables

7.2.1. Nonvariable/Variable "Variables"

Several stars from Clement's catalog were suggested to be nonvariable in Stetson et al. (2014). To start with, stars V17, V44–V48, V50, and V51, designated earlier as RR Lyrae, probably as a result of their location on the HB of the cluster's CMD, were found by Stetson et al. (2014) to be nonvariable. We also find stars V17, V45, V46, and V50 to be nonvarying in both our sets; however, stars V44 and V47 show some short-period variation, while V48 and V51 show some long-period variation (Figure 5). While these last four stars may be varying, they are not of RR Lyrae type based on the shapes of their light curves. We have plotted the light curves only in *R* band to save space.

Among the non-RR Lyrae stars (V53, V54–V60, V65, V70, V72, V75, V77, V78, and V80) that appear to be nonvariable in Stetson data or for which their variability is under serious doubt, we also find that V54, V55, V57–V60, V65, V75, and V80 are nonvariable in both of our sets to the limit of our sensitivity. We cannot comment on V53, as it was saturated in all frames.

Incidentally, stars V51, V56, and V59 were designated as secondary photometric standards (S8, S72, and S94, respectively) in Stetson's (2000) online catalog of secondary photometric standards. In fact, stars V56 and V77 deserve special mention. In 2008, a spectroscopic search for binaries in M4 was conducted on the basis of RV variations (Sommariva et al. 2009), where 57 binary candidates were identified. Stars V56 (#29065 in Sommariva et al. 2009) and V77 (#34848 in

Table 4
Data on Previously Reported Variables Obtained in This Work

Name	$P_{\rm Clement}$ (day)	Present Work (day)	$\Delta R/\Delta I$ (mag)	Type/Comments
V3	0.5067	0.50699(9)	0.326/0.533	RRab, $I > R$ amplitude
V33	0.6148	0.6136105	0.6834	RRab, R amplitude
V34	0.5548	0.55471	1.062/0.872	RRab
V36	0.5413	0.545	0.276/0.244	RRab
V40	0.3853	0.38535	0.51895/0.18834	RRc, lower star on Figure 9 (Bottom); instrumental magnitudes
V43	0.3206	0.3211	0.3232/0.25286	RRc
V44	⋯	non-var	⋯	HB
V45	⋯	non-var	⋯	HB
V46	⋯	non-var	⋯	HB
V47	⋯	LP?		HB, next to overbright (possibly variable) stars
V48	⋯	LP?	⋯	HB
V50	⋯	non-var	⋯	HB
V51	⋯	LP?	⋯	HB, ≡S8 in (1)
V54	⋯	non-var	⋯	⋯
V55	⋯	non-var	⋯	⋯
V56	⋯	LP?	⋯	≡S72 (1), RG, spectroscopic binary candidate (2)
V57	⋯	non-var	⋯	⋯
V58	⋯	non-var	⋯	⋯
V59	⋯	non-var	⋯	≡S94 (1)
V60	⋯	non-var	⋯	v
V65	0.0872	non-var	⋯	⋯
V70	0.3031	0.30315(9)	0.080/0.083	EB
V72	0.3084	0.30847	0.118/0.100	EB, BSS
V75	0.2973	non-var	v	v
V76	0.3058	0.305736	0.29979/0.23335	RRc, $V12$ in ASAS Variable Stars Catalog (3)
V77	⋯	LPV?	⋯	possible EB (4), spectroscopic binary candidate (2),
			⋯	X-ray source associations: CX5 and CX9 (5)
V78	⋯	non-var	⋯	⋯
V79	1.2472	close to 1.2	⋯	very noisy light curve
V80	⋯	non-var	⋯	⋯
SSS-NV3	⋯	0.49178(3)	0.567/0.531	RRab, SSS_J162529.2-261718 (6)
C2	⋯	0.45427(7)	0.835/0.645	RRab (4)

References. (1) Stetson (2000); (2) Sommariva et al. (2009); (3) Pojmanski et al. (2006); (4) Stetson et al. (2014); (5) Bassa et al. (2004); Kaluzny et al. (2013); (6) Torrealba et al. (2015).

Sommariva et al. 2009) (=K56 from CASE; see Section 7.1) are among this list. In Stetson et al. (2014), these stars are labeled as "EB or LPV" for V56 and "possible EB" for V77, without the periods. We cannot determine their variability type based on our light curves (Figure 5).

V56. This star was first declared as variable by Yao (1987) based on Greenstein (1939), though neither its coordinates nor its period were given in Clement et al. (2001). We found its coordinates (see above Table 2) and discovered that it coincides with Stetson's secondary photometric standard S72 (Stetson 2000). It is an RG star, based on its position on the CMD, and a cluster member. In Figure 5 we show its time-domain light curves from both telescopes.

V77 = KV56. Neither Clement et al. (2001) nor Kaluzny et al. (2013) give the period for this star. Kaluzny et al. (2013) present its time-domain light curve (their Figure 10), which looks like an LPV. It does not look variable on our C18 frames, but its T40 light curve gives an indication that it might be an LPV (Figure 5). Though it could well be decided finally as a binary based on Sommariva et al. (2009) RV variations and Stetson's conclusion, the situation is complicated by its association with X-ray sources CX5 and CX9 (Bassa et al. 2004; Kaluzny et al. 2013). Clearly, more studies have to be done to finalize the issue.

V70 and V72. V70 and V72 were found by the *HST* study (Nasimbeni et al. 2014) to vary as contact eclipsing binaries (cEBs) with periods of about 0.3 days. We also find them to be variable (Figure 6), with V72 being a BSS (see Section 7.4.2 and Figure 14, top). Interestingly, V70 is reported as RR Lyrae in the 2MASS catalog: 2MASS J16233328-2631079.

7.2.2. SX Phe Stars in M4

SX Phe variables in GCs are of particular interest because they occupy the region on the CMD that coincides with the BSS region. These stars are believed to be a result of a binary merger. With a slow start (only a handful known in the 90 s), the count now exceeds 100 in the galactic GCs, except in M4, which presents an important puzzle, especially that the cluster hosts a large number of BSSs (30 BSSs found by Rucinski 2000, and one more by Nascimbeni et al. 2014). While all SX Phe are BSSs, not all BSSs are SX Phe. Of all these BSSs, only two are found to be variable—both are eclipsing binaries of W Uma type: V72 (Kaluzny et al. 1997) and no. 7820 (Nasimbeni et al. 2014).

There are few reports of SX Phe in M4 in the literature. Yao & Uloa (1993) reported a star, which was assumed by Rodriguez & López-González (2000) as SX Phe in their

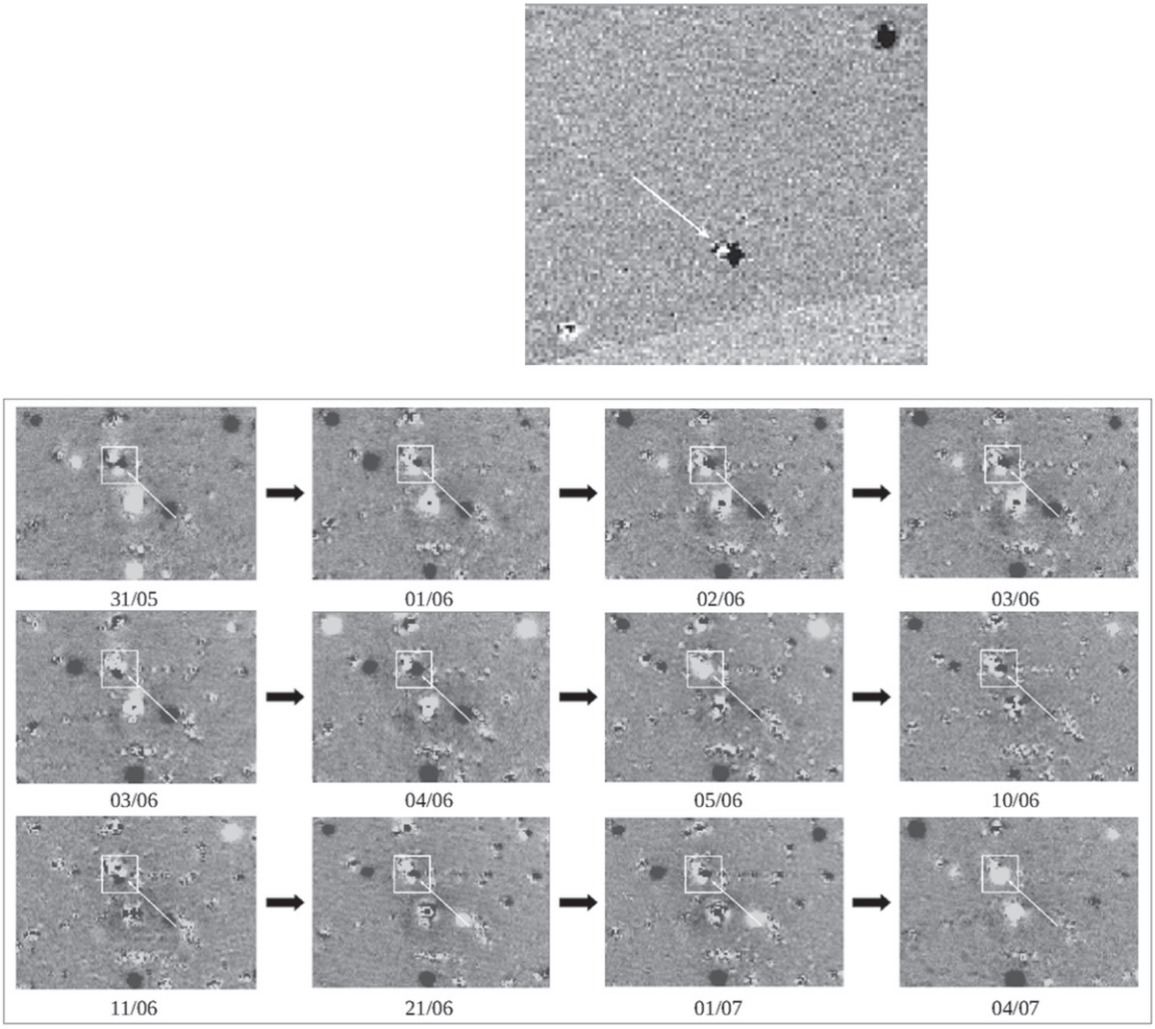

Figure 9. Top: T40 difference frames of V36 from two different nights. The white arrow points to a pair of spatially close stars (3.″6 apart); the lower star is clearly a variable. Bottom: T40 difference frames of the the V40 pair (in the white box) from May 31 (31/05) onward. It is clearly seen that both stars are variable. The angular separation is 1.″666. In the center there is a saturated star. Other variables here are V16, V18, V21, V24, and V25.

compilation of then known SX Phe stars in GCs. This star, however, was an outlier in their metallicity–period relation. The star, assigned as V48, not only does not lie in the BSS region of the cluster's CMD (in HB; Yao & Uloa 1993), but is even suggested to be nonvariable in Clement's catalog. As we mentioned in the previous subsection, it shows some irregular variation in our T40 set, but does not look variable in the C18 set. Kaluzny et al. (2013) reported four SX Phe stars, two cluster members (K61 and K68), and two nonmembers (K62 and K64). Stetson et al. (2014) reexamined Kaluzny's data and tentatively found three of those stars to be nonvariable and one —a nonmember K64—to be variable. The *HST* report by Nascimbeni et al. (2014) studied the central part of the cluster, where there should be many SX Phe stars by analogy with other low-metallicity GCs (e.g., M53, M55, or ω Cen), but found none, though they would have been able to detect the variability down to millimag amplitudes. They have detected other Kaluzny et al. (2013) variables, such as K48–K51, K53, and K66—all eclipsing binaries. Therefore, they should have been able to detect K61 and K68 as SX Phe, if genuine. We examined these stars and conclude that stars K61 and K68 are most probably not SX Phe (Table 3, Figure 7), which again brings the number of SX Phe in M4 to zero.

7.2.3. RR Lyrae Stars in M4

RR Lyrae stars in the field of M4 from several telescopes have been extensively reported (see Nasimbeni et al. 2014; Stetson et al. 2014). Here we complement that set by reporting on RR Lyrae stars that were outside those FOVs but nevertheless are associated with M4 based on their position on the cluster's CMD and their proper motion (PM).

In quad 5 of the LAIWO CCD there is a variable designated as V12 in the ASAS Variable Stars Catalog (Pojmanski et al. 2006) —an RRc, which, however, was believed to be a field variable (Lane et al. 2010). We have obtained its *R* and *I* photometry on both telescopes and suspected it to be a cluster member. First, its mean *R* and *I* magnitudes are consistent with the mean *R* and *I* magnitudes for 45 RR Lyrae in M4 of ∼12.8 and ∼12.3, respectively (Stetson et al. 2014). Second, its heliocentric radial velocity (HRV) of 64.8 km s^{-1} given in the ASAS catalog is consistent with the HRV of M4 $\approx$ 69.8 km s^{-1}. Finally, in Stetson et al. (2014) the variable V76, which did not have the

Table 5
Data on New Variables

ID	R.A.	Decl.	PPMXL[a] μ_α, μ_δ	Period (day)	$\Delta R/\Delta I$ (mag)	Epoch[b] 2455000.0+	GCVS Type/Comment
NV1	16:21:55.81	−26:13:29.0	−15.6, −6.8	≈33	0.105/0.063	846.9082	Unclassified LPV, could be 0.5046(?)
NV2	16:22:35.93	−26:19:37.2	−5.6, −6.9	46(1)	0.090/0.051	700.0000	LPV+linear trend −0.0009 mag day^{-1}, IR source 2MASS J16223585-2619365, T-Tauri-like
NV4	16:25:09.48	−26:39:42.4	−26.5, −23.1	0.34444(1)	0.328/0.309	710.3406	EW
NV5	16:24:38.66	−26:44:24.1	−3.4, −9.9	0.54457(3)	0.406/0.403	711.3890	EA, *ROSAT* X-ray source (1)
NV6	16:24:44.27	−26:46:18.4	−12.4, −24.4	0.8613(1)	0.120/0.124	711.1503	Unclassified (P = 0.4306?), HRV = −3.1 (2)
NV7	16:21:47.46	−26:09:40.5	−6.8, −12.7	0.43031(1)	0.300/0.267	711.0751	RRc/RRab, Blazhko effect?
NV8	16:24:28.41	−26:28:28.1	−1.5, −11.8	0.64783(1)	0.190/0.150	712.4039	RRc
NV9	16:22:06.35	−26:39:25.8	−16.2, −11.6	7.8	0.335/0.274	715.4	unknown
NV10	16:20:51.18	−26:36:20.5	−15.2, −11.0	0.70777(6)	0.375/0.367	711.7192	RRab, Blazhko effect
NV11	16:20:49.93	−26:36:07.9	−9.7, −4.4	0.35640(5)	0.374/0.331	710.5815	EW, O'Connell effect
NV12	16:23:35.69	−26:47:45.8	−14.1, −17.8	3.944(2)	0.153/0.156	719.3348	DCEP? Associations: *ROSAT* X-ray source 1RXS J162336.6-264747 (3) *Chandra* X-ray source CXO J162335.5-264746 (4)
NV13	16:21:26.04	−26:46:05.8	−12.5, −13.7	0.33604(1)	0.644/0.788	709.8105	RRab
NV14	16:24:59.14	−26:54:20.7	−4.4, −13.3	0.44726(2)	0.430/0.406	710.5156	EW, O'Connell effect
NV15	16:24:16.63	−26:57:14.0	−19.3, −32.1	5.091(3)	0.392/0.205	726.6111	DCEP?, HRV = −5 km s^{-3}, X-ray source 1RXS J162417.7-265717 at ∼ same location (3)
NV16[c]	16:22:57.80	−26:54:40.5	−10.59, 3.32				DSCT (multiperiodic):
				0.2477(1)	0.156	709.7545	P_1
				0.1579(1)	0.122	709.9546	P_2
				0.2114(4)	0.022	709.8627	P_3
NV17	1. 16:21:48.43	−26:50:55.0	−65, 64	1.3144(2)	0.203/0.062	713.2884	EA, Visual double star WDS J16218-2651
	2. 16:21:47.99	−26:50:47.2	−54, 66				+ high proper motion star (5)
NV18	16:22:50.63	−26:28:51.4	−32.4, −11.5	0.28054(1)	0.168/0.168	709.6490	EW, 3 close stars on C18 frames, coordinates of the most prob. one (PPMXL'10)
NV19	16:21:03.99	−26:24:35.9	−7.0, −3.0	0.226067(7)	0.138/0.138	710.7800	EW, 2 stars at 2.″136, no PPMXL, UCAC4 data, only UKIDSS J162103.99-262435.9 and PM
NV20	16:21:05.83	−26:24:15.7	−8.2, −5.6	0.112966(3)	0.081/0.042	710.5573	DSCT

Notes. *References to the additional data*: (1) M4 source #5, Ishikawa et al. (2004); (2) Lane et al. (2011); (3) Voges et al. (2000); (4) Evans et al. (2010); (5) Hartkopf et al. (2013).
GCVS (General Catalog of Variable Stars; Samus et al. 2007–2015) type is codified as follows: EW–W Ursae Majoris-type eclipsing variable; EA–Algol (Beta Persei)-type eclipsing system; DCEP—classical Cepheid, or Delta Cep-type variable; DSCT—variable of the Delta Scuti type, field analog of SX Phe variables.
[a] M4 cluster overall proper motion (PPMXL'10): μ_α − 17.9, μ_δ = −19.4.
[b] Epochs are for minimum light for eclipsing binaries and maximum light for pulsating stars.
[c] Epochs, periods, and amplitudes are only for R filter for this star.

Table 6
Data on Candidate Variables

ID	R.A.	Decl.	UCAC4# (1)	PPMXL μ_α, μ_δ	Type	Additional Data
VC1	16:22:20.0	−26:32:38.6	318-087831	−10.6, −1.6	LPV/EB	
VC2	16:22:34.8	−26:27:13.1	318-087877	−5.0, −20.5	LPV/EB	Associations: CXO J162234.8-262712 (2), X-ray/Radio source (3)
VC3	16:22:22.9	−26:24:01.9	318-087841	−6.3, 0.6		
VC4	16:22:41.35	−26:26:02.5	318-087915	−3.0, −2.0	LPV?	≡S989 (4), 2MASS J162241.4-262601 IR source (5)
VC5	16:23:33.14	−26:30:56.8	318-088763	−6.7, 41.9		no PPMXL data, PM from UCAC4.
VC6	16:22:41.54	−26:23:03.4	319-085449	−28.4, −24.9		
VC7	16:22:18.00	−26:29:11.6	no data	−8.7, −4.8		3 stars close, PPMXL data only on one star

Note. (1) Zacharias et al. (2013); (2) Evans et al. (2010); (3) Flesch (2010); (4) Stetson (2000); (5) Evans et al. (2003), c2d *Spitzer* final data release (DR4).

coordinates in Clement's catalog, was provisionally identified as RR Lyrae at a cluster distance, and the coordinates given therein coincided with the coordinates of V12. Therefore, we concur with Stetson's coordinates and confirm the designation of this star as V76, a member of M4 and an RRc variable. Its period in the ASAS Catalog is given as 0.305725 days; we find the best period as 0.305738 days and present its phased R and I light curves in Figure 8.

In addition, three variables were outside the Stetson et al. (2014) FOV: V3, V34, and V43. In Figure 8 we show their

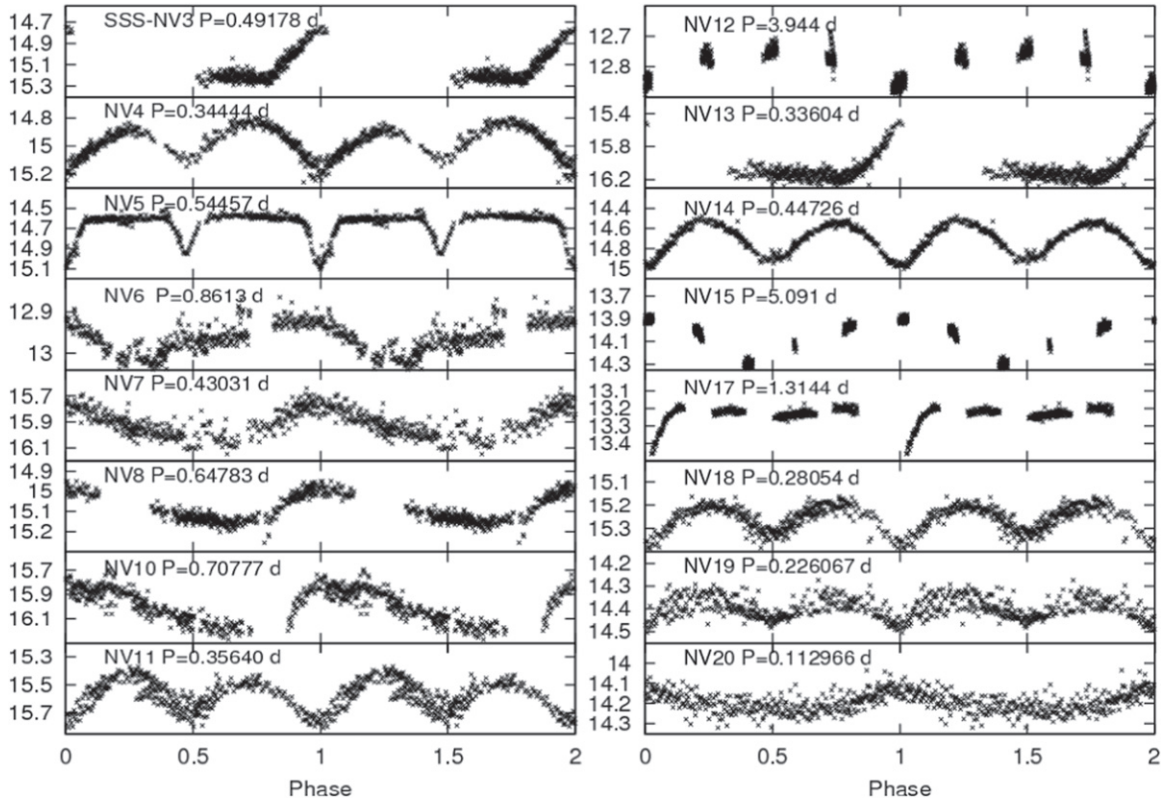

Figure 10. Phased light curves of new variables in instrumental *R* magnitudes. Names and periods are given in the plots.

light curves, phased with best found periods (Table 4). Variables V3 and V43 were outside the T40 FOV; therefore, we have only C18 light curves for them.

Variables V33 and V79 are described in Stetson et al. (2014) as having insufficient data, being located in the less well-observed outer parts of the cluster. Table 4 of Stetson et al. (2014) does not show their *R* amplitude, and no period or type for V79. That is why we show only their *R* magnitude light curves (calibrated to standard scale) in Figure 8. For V33, the period given in Clement's catalog and Stetson et al. (2014) is 0.6148(3542) days; we find the best phasing with 0.6136105 days. For V79 we only found that the period is close to ~1.2 days; in Figure 8 its light curve is phased with Clement's period (Table 4). We also cannot assign variability type to V79; it is possible that it is a multiperiodic variable.

Variable V36 is one of the pair of closely separated stars (3.″6) of equal brightness (Figure 9, top). A previous study (Stetson et al. 2014) reports noisy light curves for this star. Our T40 light curves were also quite noisy, probably due to the low cadence; therefore, we present only C18 light curves (Figure 8).

Both Stetson et al. (2014) and Nascimbeni et al. (2014) discovered that previously reported atypical RR Lyrae V40 is in fact a blend of two neighboring RRc stars of equal brightness, separated by 1.″666. In spite of the limited sensitivity of our photometry and relatively large pixel sizes, we are nevertheless able to distinguish the two stars on the difference frames, most probably due to their large amplitudes and different periods (Figure 9, bottom). This demonstrates the power of the DIA technique even in the crowded centers of GCs and our ability to detect a high-amplification event if one occurred. It was, however, more difficult to obtain high-quality light curves for these two stars because they are so close that their zero-point flux estimate could not been done correctly; the calculated zero-point flux is thus a measurement of the combined flux of these stars. Thus, we could not extract the light curves from C18 as its pixel scale is of the order of separation, and we present T40 instrumental *R* and *I* phase curves of the lower star (Figure 8).

7.3. New Variables/Variable Candidates

After examining a set of the candidate variables and rejecting obviously spurious ones, we find 19 new variable stars (Table 5 and Figure 10) and 7 candidate variables (see discussion in Section 7.5). The candidates look variable but have noisy light curves that do not allow us to certainly detect the periods or types. In addition, we also detected the C2 variable of Stetson et al. (2014), and since Stetson et al. (2014) have no *R* and *I* data for this star, we include its *R* and *I* light curves with our new detections (Figure 11, top). In Figure 10 we present phased light curves of those newly detected variables where we could find the significant period. We present here only *R* magnitudes to save space. We also include with our new detections the RRab star SSS_J162529.2-261715, reported by the Siding Spring Survey (SSS) as part of the Catalina Sky Surveys (CSSs; Torrealba et al. 2015) and available online in the CSS Data Release 2 (CSDR2[11])—at the time of our observations and analysis it was still unknown. We reserve here its nomination as NV3 with an SSS prefix. In addition, CSDR2 presents only its *V*-band light curve with rather low cadence—the best period generated by the online tool is 0.4894932 days. We complement it with our high-cadence *R*- and *I*-band

[11] http://nesssi.cacr.caltech.edu/DataRelease/

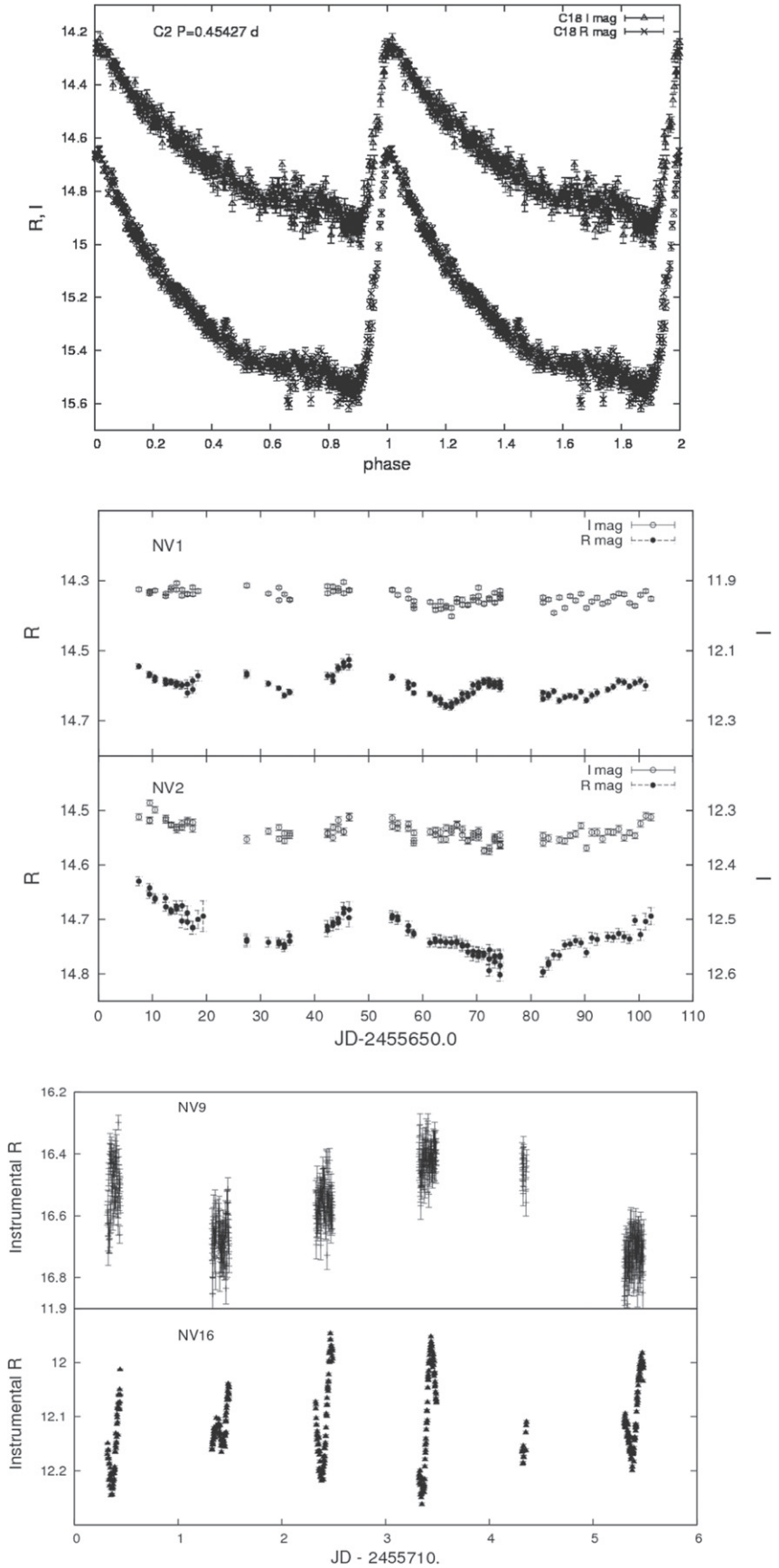

Figure 11. Top: C18 light curve of C2 in standard *R* and *I* magnitudes, phased with 0.45427(7) day period. Middle: T40 time-domain light curves of NV1 and NV2 in standard *R* and *I* magnitudes. Bottom: C18 time-domain light curves of NV9 and NV16 in instrumental *R* magnitudes.

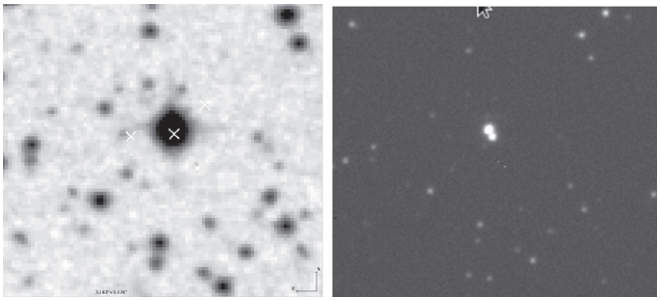

Figure 12. Field of NV12. Left: archival ESO/R/MAMA image of the field. The object is in the center. White crosses indicate the associated X-ray sources: CXO J162335.5-264746 right on the object, 1RXS J162336.6-264747 to the left of it, and 1AXG J162334-2647 to the right. Right: 30 s *V*-band JCBT image shows the object to be a visual double star with ∼2.″9 separation. The variable is most probably the lower star.

photometry (Figure 10) and update its period as 0.49178(3) days.

7.3.1. RR Lyrae

We detected six RR Lyrae: one RRc (NV8), four RRab (SSS-NV3, NV10, NV13, and C2), and one with undetermined pulsation mode (NV7). One of these stars, SSS-NV3, was reported recently in the Catalina Southern Sky Survey (J1625293-261718; Torrealba et al. 2015) as RRab with the period $P = 0.48949$ days and only *V*-band photometry. We find its period as $P = 0.49178(3)$ days and present its *R*- and *I*-band photometry. Variable C2 was detected by Stetson et al. (2014); we supplement their discovery with good-quality *R* and *I* light curves. All these RR Lyrae do not belong to the M4 cluster and are the field variables. The distances to SSS-NV3 and C2 are estimated as 4.37 (Torrealba et al. 2015) and 7.7 kpc (Stetson et al. 2014), respectively. One of the new RR Lyrae, NV10, exhibits Blazhko modulation, and for another one, NV7, the data are insufficient to firmly determine the pulsation mode.

7.3.2. Eclipsing Binaries

We find seven eclipsing binaries: two of type EA (detached) and five of type EW (contact). Of these binaries, only NV4 is a definite cluster member and a possible BSS. Two of the EW binaries, NV11 and NV14, display the O'Connell effect, where the primary and secondary maxima in the light curves have different magnitudes (Wilsey & Beaky 2009). One of the Algol-type variables, NV5, is also an X-ray source.

7.3.3. Other Types

We find four field Cepheids: two of Delta Scuti type (NV16 and NV20) and two classical Cepheids (NV12 and NV15). Both of the classical Cepheids are previously reported as X-ray sources (see next subsection). NV16 is a multiperiodic variable; therefore, we only show the time-domain light curve in *R* band in Figure 11 (bottom). We also have four unclassified variables: NV1, NV2, NV6, and NV9. The first two are most probably LPVs, where NV2 displays a light curve that resembles the light curves of T Tauri stars. It is also a reported IR source, which means that it could be a star belonging to the foreground Rho Ophiuchi star formation region. We present their time-domain light curves in both *R* and *I* filters in Figure 11 (middle). NV9 has a possible period of about of ∼7.8 days—we cannot find it more accurately as the interval of observations is shorter than the period, and the sampling is relatively sparse (Figure 11, bottom).

7.3.4. The Nature of Variable NV12

This source appears as an unresolved extended image on the C18 frames (it is outside the T40 FOV). At least three X-ray sources and several optical sources are listed within a 1′ radius circle in different catalogs (SIMBAD Astronomical Database). *Chandra* point X-ray source CXO J162335.5-264746 (Evans et al. 2010) coincides with the position of the object. *ROSAT* X-ray source 1RXS J162336.6-264747 (Ueda et al. 2001) is at ∼13.″4 to the left of it, and *ASCA* unresolved X-ray source 1AXG J162334-2647 with the MEKAL fitted spectrum (Ishikawa et al. 2004) is at ∼13″ to the right of it. An archival

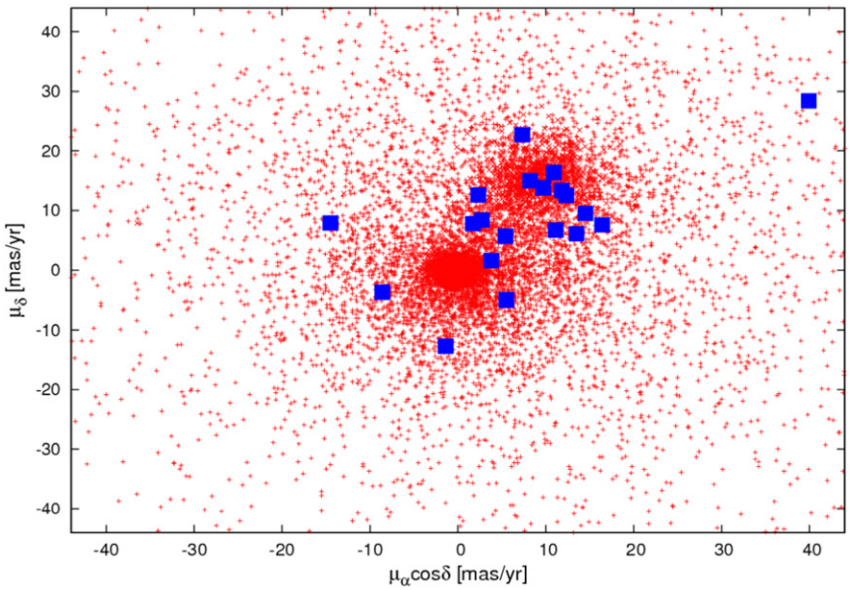

Figure 13. VPD, in equatorial coordinates, for all stars in quad 8 with available measures of PMs (PPMXL'10). Filled squares are the newly found variables.

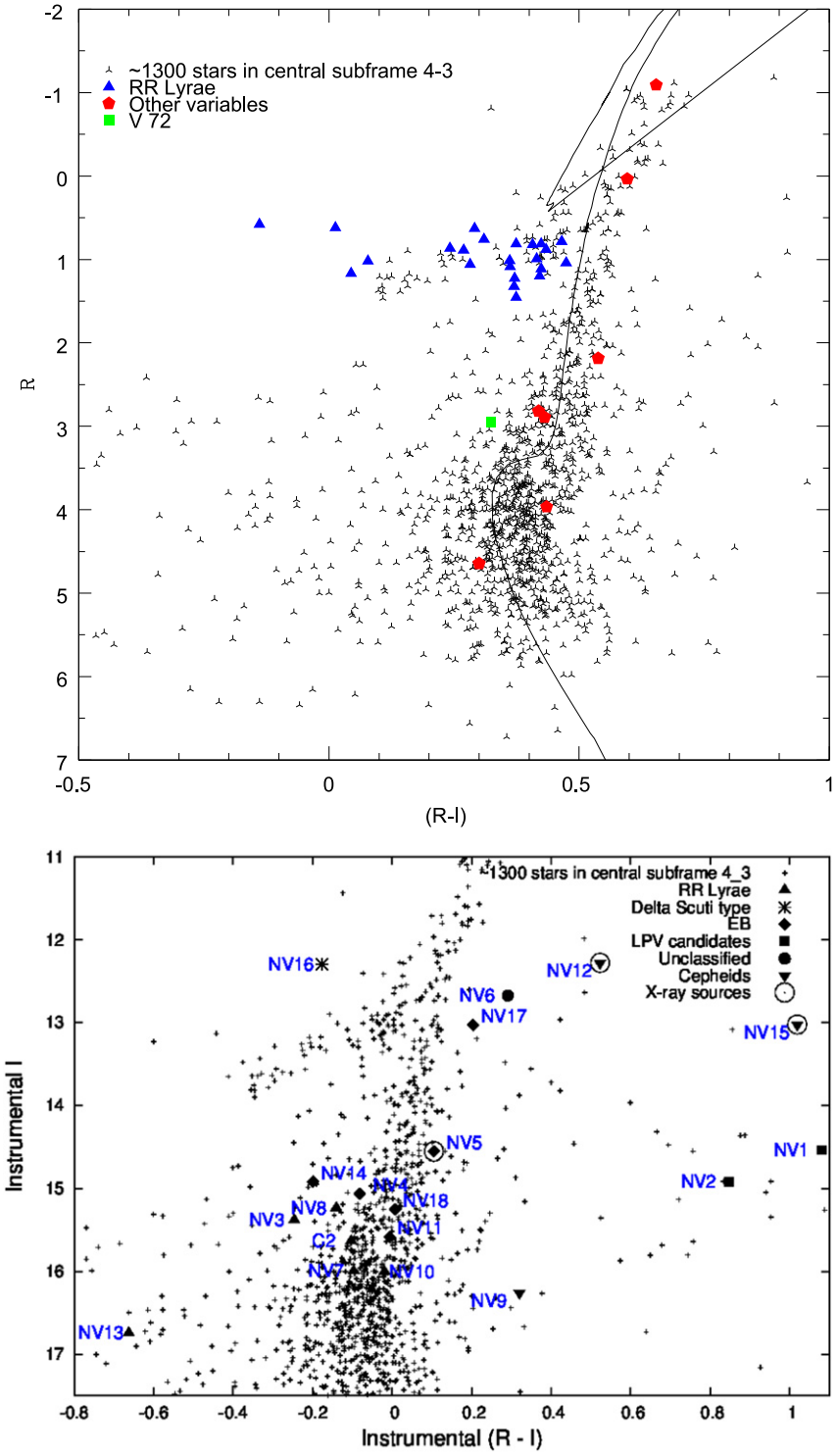

Figure 14. Top: CMD of the 4_3 subframe of the C18 central part of M4 in absolute magnitudes with known RR Lyrae and other variables located in this subframe. V72 is the BSS eclipsing binary star located in the BSS region of the CMD. Overplotted is a 12.6 Gyr isochrone from Girardi et al. (2000) with $E(B - V) = 0.27$. Bottom: CMD in instrumental magnitudes of the 4_3 subframe of the C18 central part of M4 with newly found variables. Location on the CMD aids in variable identification.

red ESO/R/MAMA image (Figure 12, left) shows an extended object at this position. Imaging from the 1.3 m JCBT telescope of the VBO (Vainu Bhappu Observatory, Tamil Nadu, India) resolved the object into the visual double star (Figure 12, right). The position of the *Chandra* X-ray source CXO J162335.5-264746 is coincident with the lowest of the two stars (Figure 12, Right). Our preliminary analysis indicates that this is probably a Delta Cep-type variable, or a classical Cepheid, which were shown in 2009 (Engle et al. 2009) to display X-ray activity representing the first true detection of X-ray emission in classical Cepheids. Incidentally, another detected DCEP, NV15, also has an X-ray source association (Table 5). Spectroscopic studies of NV12 are under way, and the results will be reported in a forthcoming paper.

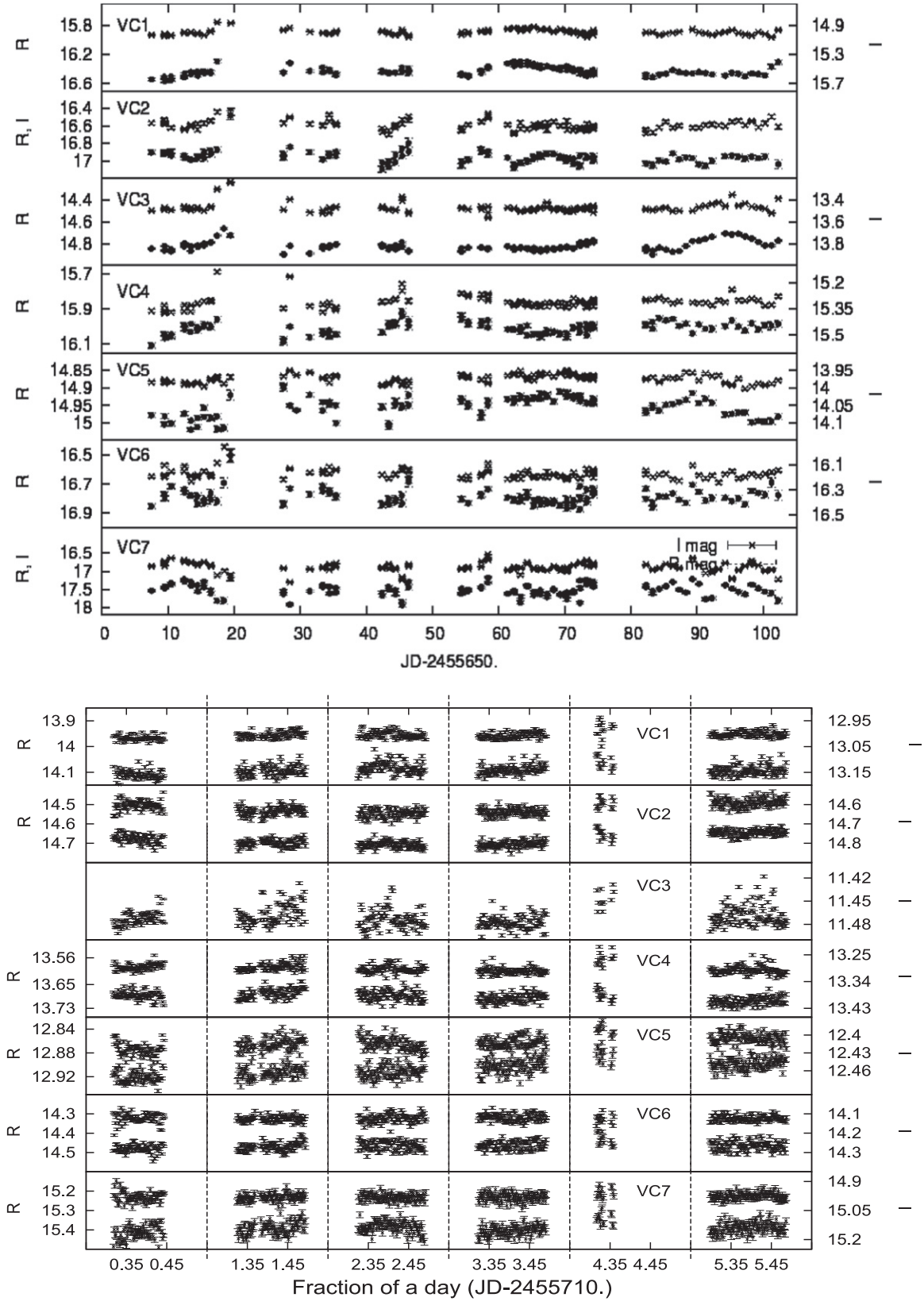

Figure 15. Time-domain light curves of candidate variables in instrumental *R* and *I* magnitudes. Top: T40 light curves; bottom: C18 light curves. Names are given in the plots. For each variable, lower curves are *R* band and upper curves are *I* band.

7.4. Cluster Membership of New Variables

7.4.1. Proper-motion Diagram

One of the ways to detect foreground/background contamination consists in identifying field stars on the basis of their PM, which usually differs from the overall cluster motion. On the vector point diagram (VPD), the zero point of the motion is the mean motion of the cluster itself, and the bulk of the stars clustered around the origin would consist mostly of cluster members, while field stars will be distributed over a larger range of PMs. To build the VPD for our sample, we have found the PPMXL'10 PM for all stars in quad 8, as well as for our newly found variables. The VPD of Figure 13 shows that the majority of the stars in quad 8 share the mean cluster motion. It also shows that most of the newfound variables are probabbly not cluster members. The possible members among the new ones are NV4, NV6, NV9, NV10, NV12, and NV13, and most certain nonmembers are NV17, NV18, NV19, and C2.

7.4.2. Color–Magnitude Diagram

To aid in identification of the newly found variables, we have constructed the CMD of the central region of M4 from C18 images (Figure 14). The RF of subSection 4_3 was astrometrically and photometrically calibrated (see Section 6). In Figure 14 we present the CMD with known variables located in this subsection; the isochrone from Girardi et al. (2000) for an age of 12.6 Gyr in absolute magnitudes is superimposed on the plot. From the sliding fit, we obtain $E(R-I)=0.22$, corresponding to the reddening $E(B-\mathrm{V})=0.27$, where total extinction in R and I bands, $A_R=2.32\,E\,(B-V)$ and $A_I=1.5\,E\,(B-V)$, respectively, were taken from Schultz & Wiemer (1975). The distance modulus 11.27 was calculated for the distance of 1.8 Kpc to M4 (e.g., Kaluzny et al. 2013). This curve matches the colors of the turnoff.

Based on the CMD, we find that out of NV4, NV6, NV9, NV10, NV12, and NV13, only NV4 (an EW star located close to the BSS region) can be firmly considered as a cluster member, with the rest most probably being foreground/background objects. However, NV12 is still a subject of study. It is possible that its C18 magnitude and colors are blended, since on C18 we could not resolve the two components.

7.5. Candidate Variables

We have selected several possible variables, whose light curves are noisy or the stars themselves are situated on the edges, where the apparent variability could have been induced artificially. For all but two we have the light curves from both telescopes. We have assigned the name VC (variable candidate) to these stars. The available data on these stars and their instrumental R and I time-domain light curves are presented in Table 6 and Figure 15, respectively.

8. CONCLUSIONS

GC M4 was observed as part of our multisite program on the search of low-mass objects in GCs by ML. We presented here the results of the 2011 observational run on two Wise Observatory (Tel Aviv, Israel) telescopes. We did not detect any variability signal that could be interpreted as an ML event with photometric variation larger than 0.1 mag. The most important factor in our data set that strongly limited the ML detection is a poor sampling cadence of observations rather than photometric limitations. Our initial proposal to obtain several data points per night was not realized due to various factors such as weather, malfunctions, clashes with other programs, etc. It is entirely possible that we have missed the event as the calculated timescale due to the FFP is of the order of a day; therefore, the statistical significance of the null detection is very low. Though no definitive ML signal was detected, we have obtained a good R and I photometry of an M4 field. We have recovered most of the variables previously reported in M4. We found the coordinates of the stars for which there were no data in Clement's catalog. We have inspected previously suspected field variable V12 (ASAS) and have identified it with the cataloged V76, obtaining its R and I light curves. We have confirmed that two previously suspected SX Phe stars in M4 do not pulsate as SX Phe, and that M4 is still void of SX Phe stars. We also obtained R and I photometry of variables not covered by Stetson et al. (2014): V3, V34, and V43. We concur with the Stetson et al. (2014) conclusion that stars V57–V60, V65, V75, and V80, previously reported as variable, are nonvariable in both our sets to the limit of our sensitivity. However, stars V70 and V72, which appear to be nonvariable in their data, are, in fact, variable, and one of them is a BSS.

Our survey resulted in detection of several new variables and variable candidates. Out of the new certain variables, however, only one (NV4) can be accepted as a cluster member, based on its PM and a CMD location. It is an eclipsing binary and also, most probably, a BSS. We have detected six RR Lyrae: one RRc, four RRab, and one whose pulsation mode cannot be yet determined based on incompleteness of our light curve. Two of these RR Lyrae were also recently reported, SSS-NV3 and C2, and we complement the reported data with R and I light curves. Some of the new variables are associated with X-ray/radio sources; one of them is Algol-type, and two are probable classical Cepheids. We also detected seven candidate variables, where variability cannot be fully confirmed on the basis of only our data. These candidates, however, look variable in the Catalina Sky Survey online data release as well (except VC5, which was not covered), but insufficient CSS temporal coverage there also does not allow us to firmly define the periods. We are looking closely into the nature of a new variable, NV12, which is associated with X-ray sources reported previously by three different missions. The results of its spectroscopic investigations will be reported in a separate communication.

All our R and I light curves from both telescopes can contribute to the completeness of the variable star database of M4, which has been started by the team of Stetson et al. (2014). Our calibrated photometry for these stars, their coordinates, and their light curves, along with the original calibrated FITS frames from both telescopes, will be available on the cloud storage and file hosting service MEGA[12] for download.[13] It is our hope that a full and complete long-baseline photometric database can be established for the GC nearest to us.

We are grateful to Wojtek Pych for providing us with the modified version of DIAPL and for his continuous help and support in its running. F.S. would like to acknowledge the support of the Simons Foundation, and the Aspen Center for Physics, where some of this work was carried out. The Aspen

[12] https://mega.co.nz/

[13] Please visit the first author's homepage at IIA for the link.

Center for Physics is supported by the National Science Foundation grant PHY-1066293. The authors thank the anonymous referee for careful and thorough reading of our manuscript and very useful comments that helped to improve the paper. This research used the facilities of the Canadian Astronomy Data Center operated by the National Research Council of Canada with the support of the Canadian Space Agency.

REFERENCES

Adamów, M., Niedzielski, A., Villaver, E., Nowak, G., & Wolszczan, A. 2012, ApJL, 754, L15
Adams, F. C., Hollenbach, D., Laughlin, G., & Gorti, U. 2004, ApJ, 611, 360
Alard, C., & Lupton, R. H. 1998, ApJ, 503, 325
Alcaino, G. 1975, A&AS, 21, 5
Allen, C., & Santillan, A. 1993, RMxAA, 25, 39
Bally, J. 2003, in ASP Conf. Ser. 287, Proc. 2002 Int. Astronomical Observatories in Chile workshop, Galactic Star Formation Across the Stellar Mass Spectrum, ed. J. M. De Buizer, & N. S. van der Bliek (San Francisco, CA: ASP), 263
Bassa, C., Pooley, D., Homer, L., et al. 2004, ApJ, 609, 755
Baumeister, H., Afonso, C., Marien, K.-H., & Klein, R. 2006, Proc. SPIE, 6269, 62693I
Beer, M. E., King, A. R., & Pringle, J. E. 2004, MNRAS, 355, 1244
Bennett, D. P., Anderson, J., Beaulieu, J., et al. 2007, arXiv:0704.0454
Bennet, D. P., Anderson, J., Beaulieu, J.-P, et al. 2010, arXiv:1012.4486
Boesgaard, A. M., Jensen, E. E. C., & Deliyannis, C. P. 2009, AJ, 137, 4949
Bonnarel, F., Fernique, P., Bienaymé, O., et al. 2000, A&AS, 143, 33
Bonnell, I. A., Smith, K. W., Davies, M. B., & Horne, K. 2001, MNRAS, 322, 859
Brosch, N., Polishook, D., Shporer, A., et al. 2008, Ap&SS, 314, 163
Buchhave, L. A., Latham, D. W., Johansen, A., et al. 2012, Natur, 486, 375
Campante, T. L., Barclay, T., Swift, J. J., et al. 2015, ApJ, 799, 170
Cassan, A., Kubas, D., Beaulieu, J.-P., et al. 2012, Natur, 481, 167
Chen, L., Hou, J. L., & Wang, J. J. 2003, AJ, 125, 1397
Clement, C. M., Muzzin, A., Dufton, Q., et al. 2001, AJ, 122, 2587
Dado, S., Dar, A., & Ribak, E. 2011, arXiv:1102.2622
Davis, D. S., Richer, H. B., Anderson, J., et al. 2008, AJ, 135, 2155
Debes, J. H., & Jackson, B. 2010, ApJ, 723, 1703
Delorme, P., Gagné, J., Malo, L., et al. 2012, A&A, 548, A26
Del Santo, M., Nucita, A. A., Lodato, G., et al. 2014, MNRAS, 444, 93
de Luca, F., & Jetzer, P. 2008, IJMPD, 17, 2305
Di Folco, E., Dutrey, A., Guilloteau, S., et al. 2014, in SF2A-2014 Proc. Annual meeting of the French Society of Astronomy and Astrophysics 135
Durand-Manterola, H. J. 2010, arXiv:1010.2735
Engle, S. G., Guinan, E., Evans, N., & DePasquale, J. 2009, BAAS, 41, 43312
Evans, I. N., Primini, F. A., Glotfelty, K. J., et al. 2010, ApJS, 189, 37
Evans, N. J., II, Allen, L. E., Blake, G. A., et al. 2003, PASP, 115, 965
Flesch, E. 2010, PASA, 27, 283
Ford, Eric B. 2014, PNAS, 111, 12616
Fregeau, J. M., Joshi, K. J., Portegies Zwart, S. F., & Rasio, F. A. 2002, ApJ, 570, 171
Gilliland, R. L., Brown, T. M., Guhathakurta, P., et al. 2000, ApJL, 545, L47
Girardi, L., Bressan, A., Bertelli, G., & Chiosi, C. 2000, A&AS, 141, 371
Gorbikov, E., Brosch, N., & Afonso, C. 2010, Ap&SS, 326, 203
Greenstein, J. L. 1939, ApJ, 90, 387
Haisch, K. E., Jr., Barsony, M., & Tinney, C. 2010, ApJL, 719, L90
Hartkopf, W. I., Mason, B. D., Finch, C. T., et al. 2013, AJ, 146, 76
Horch, E. P., Howell, S. B., Everett, M. E., & Ciardi, D. R. 2014, ApJ, 795, 60
Hurley, J. R., & Shara, M. M. 2001, BAAS, 33, 1410
Hurley, J. R., & Shara, M. M. 2002, ApJ, 565, 1251
Ida, S., & Kokubo, E. 2004, in Proc. IAU Symp. 202, Planetary Systems in the Universe, ed. A. Penny (San Francisco, CA: ASP), 159
Ishikawa, T., Ishida, M., Ishisaki, T., Ohashi, T., & Yamasaki, N. Y. 2004, PASJ, 56, 453
Jackson, B., Barnes, R., & Greenberg, R. 2009, ApJ, 698, 1357
Jetzer, P. 2015, in XIII Marcel Grossmann Meeting: On Recent Developments in Theoretical and Experimental General Relativity, Astrophysics and Relativistic Field Theories, 2075
Kaluzny, J., Thompson, I. B., & Krzeminski, W. 1997, AJ, 113, 2219
Kaluzny, J., Thompson, I. B., Rozyczka, M., & Krzeminski, W. 2013, AcA, 63, 181
Lafler, J., & Kinman, T. D. 1965, ApJS, 11, 216
Lane, R. R., Kiss, L. L., Lewis, G. F., et al. 2010, MNRAS, 406, 2732
Lane, R. R., Kiss, L. L., Lewis, G. F., et al. 2011, A&A, 530, 31
Lee, S.-W. 1977, A&AS, 27, 367
Leon, S., Meylan, G., & Combes, F. 2000, A&A, 359, 907
Lin, D. N. C., Laughlin, G., Bodenheimer, P., & Rozyczka, M. 1998, Sci, 281, 2025
Liu, M. C., Magnier, E. A., Deacon, N. R., et al. 2013, ApJL, 777, L20
Lucas, P. W., Roche, P. F., Allard, F., & Hauschildt, P. H. 2001, MNRAS, 326, 695
Maciejewski, G. 2005, PERSEA 2.01, Period Search Program for Windows., (http://www.astri.umk.pl~gm/SAVS/)
Meibom, S., Torres, G., Fressin, F., et al. 2013, Natur, 499, 55
Mochejska, B. J., Stanek, K. Z., Sasselov, D. D., et al. 2006, AJ, 131, 1090
Monaco, L., Villanova, S., Bonifacio, P., et al. 2012, A&A, 539, A157
Montalto, M., Villanova, S., Koppenhoefer, J., et al. 2011, A&A, 535, A39
Nascimbeni, V., Bedin, L. R., Heggie, D. C., et al. 2014, MNRAS, 442, 2381
Nascimbeni, V., Bedin, L. R., Piotto, G., De Marchi, F., & Rich, R. M. 2012, A&A, 541, A144
Paczyński, B. 1994, AcA, 44, 235
Parker, R. J., & Quanz, S. P. 2012, MNRAS, 419, 2448
Peña Ramírez, K., Béjar, V. J. S., Zapatero Osorio, M. R., Petr-Gotzens, M. G., & Martín, E. L. 2012, ApJ, 754, 30
Peña Ramírez, K., Zapatero-Oserio, M. R., Béjar, V. J. S., Rebolo, R., & Bihain, G. 2011, A&A, 532, A42
Pojmanski, G., Maciejewski, G., Pilecki, B., & Szczygiel, D. 2006, yCat, 2264, 0
Press, W. H., Teukolsky, S. A., Vetterling, W. T., & Flannery, B. P. 2002, Numerical Recipes in C++: The Art of Scientific Computing (3rd ed.; Cambridge: Cambridge Univ. Press)
Richer, H. B., Fahlman, G. G., Brewer, J., et al. 2004, AJ, 127, 2771
Richer, H. B., Ibata, R., Fahlman, G. G., & Huber, M. 2003, ApJL, 597, L45
Roberts, L. C., Jr., Tokovinin, A., Mason, B. D., et al. 2015, AJ, 149, 118
Rodriguez, E., & López-González, M. J. 2000, Della Scuti Star Newsl, 14, 33
Roell, T., Neuhäuser, R., Seifahrt, A., & Mugrauer, M. 2012, A&A, 542, A92
Röser, S., Demleitner, M., & Schilbach, E. 2010, AJ, 139, 2440
Rosotti, G. P., Dale, J. E., de Juan Ovelar, M., et al. 2014, MNRAS, 441, 2094
Rucinski, S. M. 2000, AJ, 120, 319
Safonova, M., & Stalin, C. S. 2010, NewA, 15, 450
Samus, N. N., Durlevich, O. V., Goranskij, V. P., et al. 2007–2015, General Catalogue of Variable Stars (Samus+ 2007–2015) VizieR On-line Data Catalog: B/gcvs, http://www.sai.msu.su/gcvs/gcvs/
Schultz, G. V., & Wiemer, W. 1975, A&A, 43, 133
Schwarzenberg-Czerny, A. 1989, MNRAS, 241, 153
Skrutskie, M. F., Cutri, R. M., Stiening, R., et al. 2006, AJ, 131, 1163
Soker, N., & Hadar, R. 2001, MNRAS, 324, 213
Soker, N., & Hershenhorn, A. 2007, MNRAS, 381, 334
Sommariva, V., Piotto, G., Rejkuba, M., et al. 2009, A&A, 493, 947
Spurzem, R., Giersz, M., Heggie, D. C., & Lin, D. N. C. 2009, ApJ, 697, 458
Stetson, P. B. 2000, PASP, 112, 925
Stetson, P. B., Braga, V. F., Dall'Ora, M., et al. 2014, PASP, 126, 521
Stevenson, D. J. 1998, Natur, 392, 497
Strigari, L. E., Barnabè, M., Marshall, P. J., & Blandford, R. D. 2012, MNRAS, 423, 1856
Sumi, T., Kamiya, K., Bennett, D. P., et al. 2011, Natur, 473, 349
Sutherland, W. 1999, RvMP, 71, 421
Torrealba, G., Catelan, M., Drake, A. J., et al. 2015, MNRAS, 446, 2251
Ueda, Y., Ishisaki, Y., Takahashi, T., Makishima, K., & Ohashi, T. 2001, ApJS, 133, 1
Veras, D., & Raymond, S. N. 2012, MNRAS, 421, L117
Veras, D., Wyatt, M. C., Mustill, A. J., Bonsor, A., & Eldridge, J. J. 2011, MNRAS, 417, 2014
Voges, W., Aschenbach, B., Boller, T., et al. 2000, yCat, 9029, 0
Weldrake, D. T. F., Sackett, P. D., & Bridges, T. J. 2007, in Transiting Extrapolar Planets Workshop 366, 289
Weldrake, D. T. F., Sackett, P. D., & Bridges, T. J. 2008, ApJ, 674, 1117
Wilsey, N. J., & Beaky, M. M. 2009, SASS, 28, 107
Wozniak, P. R. 2000, AcA, 50, 421
Yao, B.-A. 1987, Msngr, 50, 33
Yao, B.-A. 1993, IBVS, 3836, 1
Yao, B., & Uloa, C. 1993, IBVS, 3846
Zacharias, N., Finch, C. T., Girard, T. M., et al. 2013, AJ, 145, 44
Zapatero-Oserio, M. R., Béjar, V. J. S., Martín, E. L., et al. 2002, ApJ, 578, 536